Review in Advance first posted online on August 7, 2013. (Changes may still occur before final publication online and in print.)

Numerical Simulation of Flowing Blood Cells

Jonathan B. Freund

Department of Mechanical Science and Engineering and Department of Aerospace Engineering, University of Illinois at Urbana-Champaign, Urbana, Illinois 61801; email: jbfreund@illinois.edu

Annu. Rev. Fluid Mech. 2014. 46:67–95

The *Annual Review of Fluid Mechanics* is online at fluid.annualreviews.org

This article's doi:
10.1146/annurev-fluid-010313-141349

Keywords

microcirculation, Stokes flow, particulate suspensions, computational biofluid mechanics

Abstract

The cellular detail of blood is an essential factor in its flow, especially in vessels or devices with size comparable to that of its suspended cells. This article motivates and reviews numerical simulation techniques that provide a realistic description of cell-scale blood flow by explicitly representing its coupled fluid and solid mechanics. Red blood cells are the principal focus because of their importance and because of their remarkable deformability, which presents particular simulation challenges. Such simulations must couple discretizations of the large-deformation elasticity of the cells with the viscous flow mechanics of the suspension. The Reynolds numbers are low, so the effectively linear fluid mechanics is amenable to a wide range of simulation methods, although the constitutive models and geometric factors of the coupled system introduce challenging nonlinearity. Particular emphasis is given to the relative merits of several fundamentally different simulation methods. The detailed description provided by such simulations is invaluable for advancing our scientific understanding of blood flow, and their ultimate impact will be in the design of biomedical tools and interventions.

1. BACKGROUND

Lysis: the destructive compromise of cell integrity

Blood at physiologic conditions is a dense suspension of cells and other formed bodies, dominated in terms of its dynamics by red blood cells, its most populous constituent. They make up over approximately 40% of the systemic blood volume in humans and vastly outnumber the white blood cells (about 1,000:1) and platelets (about 15:1). In most cases, they are the blood component principally responsible for its rheology.

This review focuses on numerical simulation of the cell-scale flow mechanisms of blood, particular its flow in vessels or devices with size comparable to the cell dimension (∼8 μm). Blood cell mechanics and microcirculatory hemorheology have been extensively reviewed (Chien 1987, Cokelet 1980, Guido & Tomaiuolo 2009, Kamm 2002, Lipowsky 2005, Popel & Johnson 2005, Secomb 2003), and blood is a specific example of particulate suspensions, which have also been extensively reviewed (Cox & Mason 1972, Guazzelli & Morris 2012, Happel & Brenner 1965, Leal 1980, Stickel & Powell 2005). The present article focuses on detailed cell-level numerical simulation of blood. The mechanics are intricate and experimental diagnostics challenging, which makes numerical simulation particularly attractive. Secomb et al. (2008) defined a spectrum of microcirculation modeling approaches; my focus is on simulations that explicitly represent cells in detail based on independently determined material model inputs.

There are several, now well-documented and thoroughly investigated, physiologic processes that depend fundamentally on the cellular character of blood. Most famously, the mean flow in small vessels becomes blunted and the effective viscosity drops to a minimum for vessel diameters $D \approx 7$ μm because of its cellular makeup (Fåhræus & Lindqvist 1931). Such behavior provides a convenient validation target for simulations to reproduce, but the future utility of such simulations is far broader. Some specific examples include gas transport (Popel 1989, Pozrikidis 2009); interactions of red and white blood cells (Freund 2007, Schmid-Schönbein 2006); platelet transport (Zhao et al. 2012), activation (Jackson et al. 2009), and adhesion (Mody & King 2008), which lead to both beneficial and harmful clotting; and the mechanical removal of aged (so-called senescent) cells by the spleen (Deplaine et al. 2011, Freund 2013) (animations of several such configurations are provided in the **Supplemental Appendix**; follow the **Supplemental Material link** from the Annual Reviews home page at **http://www.annualreviews.org**). Several pathologies are symptomatic and even deadly in large part because of the mechanical changes wrought on the red blood cells, with the global killer malaria and sickle-cell disease the two most-cited examples (Suresh 2006).

Perhaps the greatest need for the simulation of blood as a cellular suspension is in the design of micrometer-scale devices to process it at the cell scale (Abkarian et al. 2008, Toner & Irimia 2005). Some recently reported devices are designed to separate blood plasma from small samples (Homsy et al. 2012), identify and remove malaria-infected cells (Kim et al. 2012), supplant current large-scale and expensive technology to perform complete blood counts (Han et al. 2012, Layton et al. 2012), and perform label-free isolation of stiff red cells and white cells (Yang et al. 2012). All such devices depend on the behavior of often densely packed flexible cells in high-strain-rate flows and in configurations in which detailed experimental diagnostics remain challenging. The deformability of the red blood cells in such a device can be particularly important, as the means either of identifying the different cells for sorting or for avoiding excessive deformations leading to lysis. Cell lysis and harmful platelet activation are impediments to the widespread use of blood pumps (Deutsch et al. 2006), including artificial hearts (Dasi et al. 2009), the optimal design of which is expected to similarly benefit from cell-scale simulation tools. Cancer tumor growth, metastasis, and treatment with targeted agents often involve cell-scale fluid mechanics and would therefore also benefit from better simulation tools (Koumoutsakos et al. 2013). We can similarly anticipate their utility in the design of blood substitutes (Chang 2010).

2. FLOW REGIME

Blood cells have dimension $d \lesssim 10$ μm and are usually suspended in plasma with viscosity $\mu = 1.2$ Pa • s, so for physiologic flow at speeds $\lesssim$1 mm/s, Reynolds numbers are $Re \lesssim 0.01$. Thus flows are viscosity dominated even in vessels 10 times the cell size. In larger vessels, inertia becomes more significant, but homogeneous-fluid continuum models likewise become more applicable and are generally more useful. Cell-scale effects are potentially important in small regions of even high-Reynolds-number blood flows, but in such cases the local environment of a cell remains predominantly viscous.

Even the slowest physiologic flows can be expected to significantly distort the flexible red blood cells, making their distortion an essential feature of the mechanics. For velocity difference ΔU across a cell of linear dimension d, a viscous deformation stress scale is

$$\Sigma_{\text{flow}} = \frac{\mu \Delta U}{d}. \tag{1}$$

This is resisted by elastic stresses in the cell, which are complex but should scale as

$$\Sigma_{\text{cell}} = \frac{E_s \delta \ell}{d^2}, \tag{2}$$

where $E_s \approx 5$ μN/m is a membrane shear modulus (see Section 3.2) and $\delta \ell / d$ is the strain, the change in size relative to d. For $\Delta U = 1$ mm/s, a high strain of $\delta \ell / d = 0.24$ is thus anticipated. **Figure 1*a*,*b*** shows cells at rest in their nominal biconcave shapes and significantly distorted cells in flow. Simulating the details of such distorted cells as they pack closely and flow in complex geometries, such as the vessel network in **Figure 1*c***, is the principal challenge of the cellular simulation of blood.

White blood cells have an internal viscosity thousands of times that of blood (Hochmuth et al. 1993, Kamm 2002, Marella & Udaykumar 2004) and thus do not deform nearly so much as red blood cells under the same flow conditions. Platelets are similarly rigid, at least relative to the red blood cells that transport them (Mody & King 2008, Zhao et al. 2012). Mechanical or biochemical triggers can activate white blood cells (Schmid-Schönbein 2006) and platelets (Mody & King 2008), which then display complex and biochemically coupled behavior. Their subsequent mechanical interactions are fascinating and important but beyond the scope of this review.

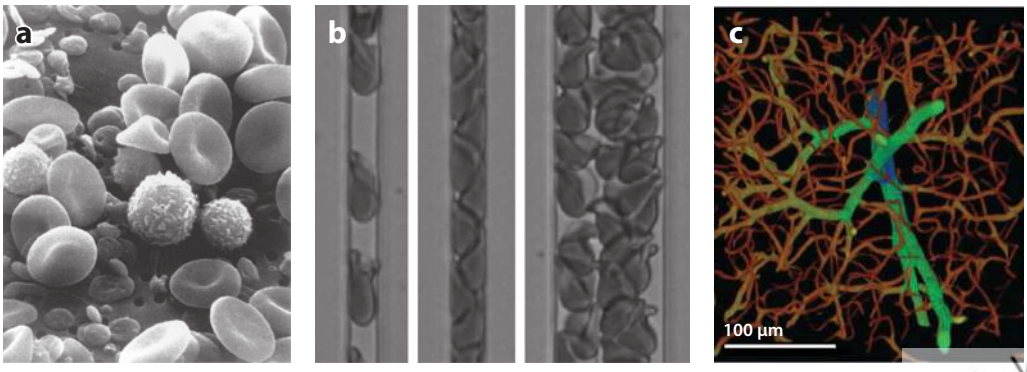

Figure 1

(*a*) Red and white blood cells and platelets at rest (Wetzel & Schaefer 1982) and (*b*) red blood cells flowing in a microfluidic device (Burns et al. 2012). (*c*) A mouse brain microvasculature scan showing its intricate geometry (Mayerich et al. 2011).

Glycocalyx: extracellular polymeric material lining vessels and red blood cells

Red blood cells are large enough that their thermal diffusion is typically negligible (Higgins et al. 2009), although blood components like platelets or small particles, such as therapeutic nanometer-scale magnetic particles, might have a more significant thermal transport under some conditions (Freund & Shapiro 2012). Red blood cell membranes, however, have bending moduli in the range of 5 to $50k_BT$, where k_B is the Boltzmann constant and T is the temperature, so their thermal fluctuations can be observed and even used to deduce material properties (Park et al. 2010). For a healthy cell at rest, instantaneous membrane deflections are $\lesssim$200 nm (Park et al. 2010) and therefore are not expected to significantly affect dynamics at the ~10-μm cell scale, except perhaps for particularly close interactions.

It is, in some cases, important to include molecular forces, which can be comparable to the fluid mechanical forces on the cells. Indeed, red blood cell aggregation (Cokelet 1980, Popel & Johnson 2005) and white blood cell (Krasik et al. 2008, Schmid-Schönbein 2006) and platelet (Mody & King 2008) adhesion occur when molecular forces exceed flow forces. However, these interactions are over $\lesssim$100−nm molecular scales, which are so much smaller than the cell scale that they in principle can be represented independently of the flow solution. I therefore do not discuss these effects in regards to simulation.

3. RED BLOOD CELL MECHANICS

3.1. Red Blood Cell Structure

Red blood cells, compared with other cells, are particularly simple in their structure (**Figure 2**). They are defined by a thin lipid bilayer membrane, coated with an ~6-nm-thick glycocalyx (Linss

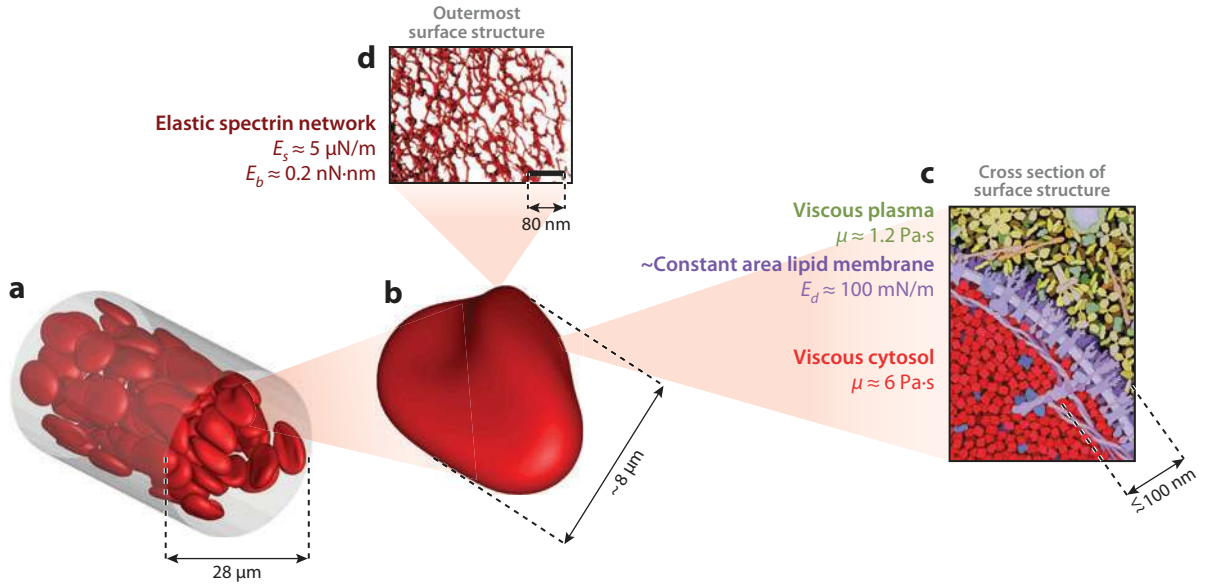

Figure 2

Flowing blood in a model vessel (*a*) involves significant deformation of the individual cells (*b*). The viscous flow, both in the interior cytosol and in the surrounding plasma (*c*), couples with the relatively weak shear and bending resistance of the membrane-associated selectin cytoskeleton (*d*), the relatively strong dilatation resistance of the lipid membrane (*c*), and the net viscous resistance of the membrane (not labeled). Panels *a* and *b* are simulation results; panel *c* is an illustration by David S. Goodsell, Scripps Research Institute; and panel *d* is a three-dimensional cryo-electron tomographic image of a native (unstretched) spectrin network (Nans et al. 2011).

et al. 1991). From within, the lipid layer is buttressed by a network of spectrin filaments that is seen to be anchored in an approximately triangular mesh when the cytoskeleton is expanded. However, in its natural, unspread state, this underlying pattern is difficult to discern (**Figure 2*d***). The combined thickness of these layers, based on atomic-force microscopy, is less than 100 nm (Heinrich et al. 2001, Nans et al. 2011), which justifies a thin shell model for their mechanical representation on the cell scale. Early in their development, red blood cells eject their nucleus and other organelles, leaving their cytoplasm as an approximately homogeneous hemoglobin cytosol (**Figure 2*c***) with Newtonian viscosity about five times that of the plasma (Cokelet & Meiselman 1968).

Cytoskeleton: the structural components of a cell; its skeleton

Cytoplasm: the material within the cell membrane

Cytosol: the liquid content of a cell's cytoplasm

3.2. Constitutive Modeling Challenge

It is thought that the lipid membrane provides a nearly incompressible envelope for the cytosol, whereas the spectrin network provides the cell its elastic resistance to shear and bending deformation (Mohandas & Evans 1994). However, given the underlying molecular complexity, there should be no expectation that any particular constitutive model could accurately represent all potential cell deformations. Adding to this challenge, membrane properties change significantly with age (Bronkhorst et al. 1995, Linderkamp & Meiselman 1982), disease (Suresh 2006), and temperature (Chien 1987). The membrane is also out of equilibrium at physiologic conditions, as evidenced by its mechanical sensitivity to ATP concentration (Hochmuth & Waugh 1987, Park et al. 2010, Yoon et al. 2008).

As with most complex materials, the best option seems to be models selected and calibrated for particular circumstances. Ideally, the corresponding measurements should be designed to parameterize particular subcomponents of proposed models, but experimental challenges have limited such an approach for red blood cells. Humphrey (2002) provided a clear discussion of these issues for constitutive modeling of tissues. For red blood cells, calibration typically follows a scattered approach, which in the end limits the fidelity of models and leaves considerable uncertainty regarding their range of applicability. Understanding these issues is important to anticipate the reliability of simulations. I first summarize the experiments available to support these efforts.

3.3. Experimental Measurements of Red Blood Cell Properties

The membrane resistance is most easily discussed in terms of reported moduli for shear (E_s), bending (E_b), dilatation (E_d), and membrane viscosity (η_m), although these are not necessarily constant, and the linear constitutive model they imply is almost certainly insufficient to provide a complete description (e.g., Yoon et al. 2008). Still, it is a reasonable starting point and is probably sufficient for many flow simulation objectives involving red blood cells. In reality, there is at present little choice in taking this approach as only a few measurements provide sufficient data to parameterize more refined models.

The earliest measurements designed to close specific constitutive models involve the aspiration of cells into micrometer-scale pipettes (e.g., Evans & La Celle 1975). For shear resistance, these measurements suggest E_s in the range of 4 to 10 μN/m. Similar micropipette results have been interpreted to deduce relatively weak bending moduli ($E_b = 0.18$ nN · nm; Evans 1983) and strong dilatation moduli ($E_d = 450$ mN/m; Evans & Waugh 1977) that indicate stiff resistance to area change. More recent measurements with optical tweezers (Dao et al. 2003), adhered magnetic bead cytometry (Puig-de-Morales-Marinkovic et al. 2007), and microrheometry based on the thermal fluctuations of cell shape (Park et al. 2010) do not significantly change these early estimates of E_s, although some suggest that the bending and dilatation moduli are significantly smaller (see **Supplemental Table 1** for experimentally deduced moduli). The complex microstructure and

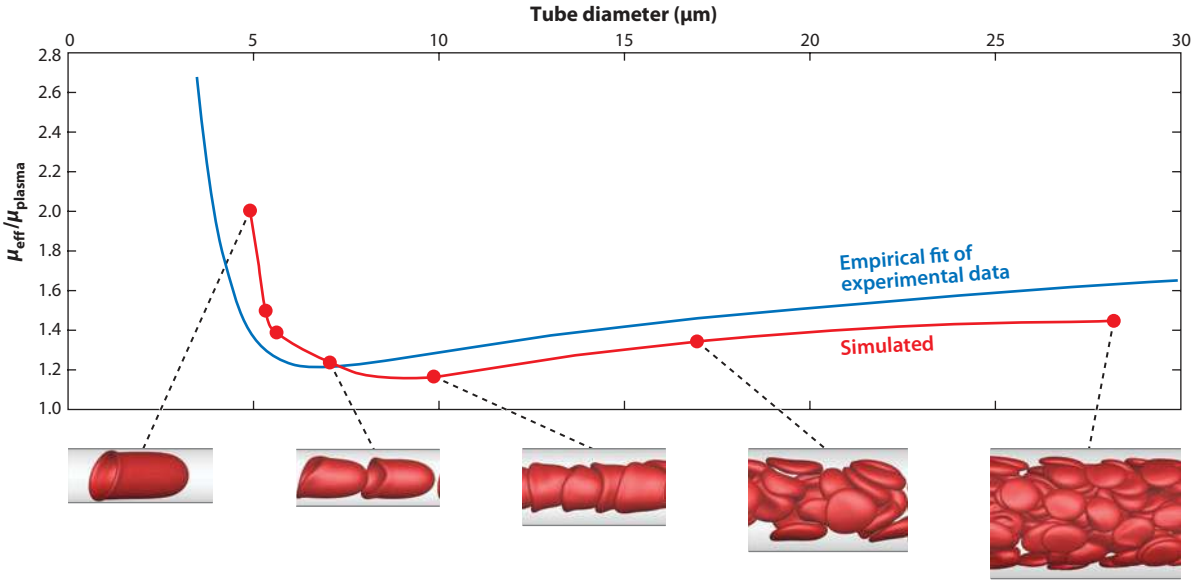

Figure 3

Simulated effective Newtonian-fluid Poiseuille-flow viscosity versus tube diameter (*symbols*) for hematocrit $H_c = 0.30$ (*red line*). The blue line is an empirical fit through a wide range of experimental data (Pries et al. 1992). Figure reprinted with permission from Zhao et al. (2010).

the diverse regimes accessed by the different experiments might partly explain the apparent scatter in the data reviewed here. This does not point necessarily to a deficiency of the experiments or even the respective constitutive models. However, it does provide a clear indication that care must be taken in applying any particular model much beyond its calibrated behavior.

Plastic deformations (Evans & Hochmuth 1976b), lysis, shear-induced tether formation (Hochmuth et al. 1973), cell aging (Bronkhorst et al. 1995, Linderkamp & Meiselman 1982), and disease (Suresh 2006) all require further model development and parameterization. For some of these cases, only minimal data are available. New measurements, perhaps aided in part by inverse simulation methods, will facilitate this development.

Most measurements involve an applied deformation of the cells, and it remains unclear which measurement technique would best correspond to the deformation experienced by flowing cells under physiologic conditions. The parameters selected by Pozrikidis (2005) based on the micropipette experiments reviewed by Skalak et al. (1989) have been used without additional calibration, for example, by Zhao et al. (2010) to reproduce reasonably well an effective viscosity curve (**Figure 3**), but there should be no expectation that these parameters or the particular constitutive model used is universal.

There is conflicting evidence concerning the importance of membrane versus cytosol viscosity in providing dissipation, although both are undoubtedly important in particular cases. Dissipation in early micropipette studies was assumed to be dominated by membrane viscosity (Evans & Hochmuth 1976a). However, the scaling arguments invoked to justify this were incomplete: A length scale alone cannot formally indicate the relative importance of two unknown viscous dissipation mechanisms. Indeed, more recent thermal flicker experiments have suggested that membrane viscosity is negligible (Park et al. 2010). It has been observed that the membrane-associated proteins remodel in a pipette (Discher et al. 1994), which might lead to greater dissipation than is

observed with mild contact-free optical-tweezer-induced deformation (Bronkhorst et al. 1995). Membrane viscosity is often neglected for convenience in simulations (Freund & Orescanin 2011, Pozrikidis 2005, Reasor et al. 2012, Yazdani & Bagchi 2011, Zhao et al. 2012), although not always (Fedosov et al. 2010, 2012). Its challenge is revisited in Section 7.2.

3.4. Modeling Approaches

With no expectation that any practical constitutive model can accurately represent the full range of conceivable red blood cell behaviors, particular simulation objectives in part will guide model selection. We can anticipate that some phenomena of interest demand only accurate representation for relatively small deformations, perhaps in rheological studies under ordinary shear rates (Doddi & Bagchi 2009, MacMeccan et al. 2009, Pan et al. 2011, Zhao et al. 2012), whereas more detailed models might be necessary to reproduce the more extreme distortions, for example, in spleenic slits (Freund 2013) or small capillaries (Freund & Orescanin 2011, Pozrikidis 2005, Secomb et al. 1986). There are two basic approaches for pursuing this: one more traditional, founded on continuum mechanics, and another that explicitly represents the microstructure.

3.4.1. Continuum modeling. A continuum model has the advantage that it is compatible with a vast set of available solution techniques, but as a fit of data, it also carries the risk that any particular model is restricted to a narrow range of conditions similar to those used for its parameterization.

Elastic stresses depend on the deformed shape of the membrane $\mathbf{x}$ relative to a reference shape $\mathbf{X}$, which can be represented by the deformation gradient tensor

$$\mathbf{F} = \frac{\partial \mathbf{x}}{\partial \mathbf{X}}. \tag{3}$$

Solid-body components of this deformation $\mathbf{R}$ are removed via the polar decomposition theorem, $\mathbf{F} = \mathbf{V} \cdot \mathbf{R}$, so the stresses can be determined from the strains $\mathbf{V}$ via the one-point left Cauchy-Green tensor

$$\mathbf{B} = \mathbf{F} \cdot \mathbf{F}^T = \mathbf{V}^2, \tag{4}$$

which describes the strain in the deformed configuration. (Alternatively, the right Cauchy-Green tensor references the undeformed configuration: $\mathbf{C} = \mathbf{F}^T \cdot \mathbf{F}$.) At physiologic conditions, deformations are large enough that finite-deformation constitutive models built in this fashion seem necessary. For an isotropic membrane, the stress depends only on the tensor invariants of $\mathbf{B}$: $I_B = \lambda_1^2 + \lambda_2^2 + \lambda_3^3$, $II_B = \lambda_1^2\lambda_2^2 + \lambda_1^2\lambda_3^2 + \lambda_2^2\lambda_3^2$, and $III_B = \lambda_1^2\lambda_2^2\lambda_3^2$, where λ_i are the principal stretches, the eigenvalues of both $\mathbf{B}$ and $\mathbf{C}$. An example of a general algebraic strain energy is

$$W = \sum_{lmn} A_{lmn}(I_B - 3)^l (II_B - 3)^m (III_B - 1)^n, \tag{5}$$

in which coefficients A_{lmn} are material properties and in general must be determined from experimental data (Ogden 1997). The algebraic form of Equation 5 is a common starting point, although many biomaterials are better fitted by exponential or other strain-energy functionals (Humphrey 2002). An isotropic model seems reasonable, assuming that the microscopic details of the spectrin network are averaged sufficiently, although measurements do suggest some structural variation (Nans et al. 2011).

A neo-Hookean strain energy $W = A_{100}(I_B - 3)$ is the simplest finite-deformation model, but its single parameter A_{100} cannot represent both the weak resistance to shear and the strong, but finite resistance to areal deformation of a red blood cell membrane. Skalak et al. (1973) recrafted

the invariants as formulated on a two-dimensional manifold to distinguish these effects:

$$I_1 = \lambda_1^2 + \lambda_2^2 - 2 \quad \text{and} \quad I_2 = \lambda_1^2 \lambda_2^2 - 1, \tag{6}$$

which are tensor invariants of a corresponding two-dimensional system or, equivalently, $I_B - 3$ and $III_B - 1$ for $\lambda_3 = 1$. The strain energy he postulated,

$$W = \frac{A_1}{4}\left(\frac{1}{2}I_1^2 + I_1 - I_2\right) + \frac{A_2}{8}I_2^2, \tag{7}$$

has the property that in the linear limit, A_2 contributes only to dilatational resistance, which facilitates calibration. Full expressions for the derivatives of W that provide the stresses are available from various sources (Barthès-Biesel & Rallison 1981, Humphrey 2002, Pozrikidis 2005, Skalak et al. 1973). The Skalak model is widely used for cellular blood flow simulation, but it can be expected to be accurate only when data are available for determining its coefficients, and its range of utility once parameterized is difficult to anticipate. For a single red blood cell suspended in a sheared flow, Pozrikidis (2005) noted only minor differences between Equation 7 and a neo-Hookean model modified to strongly resist areal deformations.

This approach can be easily extended to include more material parameters, either by retaining more terms in Equation 5 or by assuming alternative W forms. Using both volume ($\lambda_1\lambda_2\lambda_3 = 1$) and membrane ($\lambda_1\lambda_2 = 1$) incompressibility constraints, Mills et al. (2004) added a second term to the neo-Hookean model $W = A_{100}(I_B - 3) + A_{300}(I_B - 3)^3$ to better match optical-tweezer data. However, it remains unclear what flow conditions warrant such a modification. The utility of refining constitutive models depends on simulation needs, which are difficult to anticipate. Simulations of cellular flow mechanics under physiologic conditions do not seem at present to be limited by insufficient constitutive model accuracy or generality, although more extreme flow conditions are likely to test their limits. Refined continuum models will be most successful if they are developed in conjunction with experiments that isolate particular effects.

3.4.2. Discrete microstructure modeling. A complementary approach is to explicitly include microstructural detail in the model, with the expectation that this more fundamental design will make it accurate away from calibration points. Such a description, founded in molecular details, is also a starting point for coupling with the biochemistry of disease processes (Suresh 2006).

For red blood cells, this approach builds on the paradigm established by Boal et al. (1992). The spectrin network (**Figure 2*d***) is modeled by chains of beads augmented with steric and membrane-fluid forces that prevent their collapse. With this approach, Li et al. (2005) constructed a model that represents all 10^5 spectrin links in a typical cell, which reproduces observed macroscopic elastic resistance, although not necessarily as well as a third-order hyperelastic model. Representation of an entire cell this way, however, is probably unnecessary for most objectives. This has led to a series of coarse-graining efforts (Discher et al. 1998) that have reproduced, for example, both the aspiration length versus pressure behavior observed by Waugh & Evans (1979) and the microstructural remodeling observed by Discher et al. (1994).

Further coarse graining can increase utility, especially for cases in which larger numbers of cells need to be represented. Based on the Discher et al. (1998) model, Pivkin & Karniadakis (2008) identified a transform that preserves linear shear and bending resistance as spectrin-link lengths are increased, thereby reducing the number of degrees of freedom that demand explicit representation. The computational cost can be reduced tremendously by this approach, facilitating the simulation of large numbers of cells. This method is robust, even for obviously under-resolved surface shapes, and the only obvious restriction seems to be the fidelity of the geometric representation of the cell shapes (Fedosov et al. 2010).

Mathematical limits can be used to develop continuum models from discrete models, which is done in the hope of grounding their parameters in more fundamental microstructural properties rather than fitting to limited experimental data. At its simplest, this approach can predict linear moduli (Boal et al. 1992), although analysis can provide more complex models still grounded in microstructural mechanics. For example, the virial theorem has been used by Dao et al. (2006) to build a worm-like chain coarse-grained model (e.g., Discher et al. 1998) into explicit expressions for key parameters, such as the shear viscosity. A more formal approach, with the same objectives, was pursued by Hartmann (2010), employing theories that guarantee the stability of the resulting continuum model. They developed a strain-energy expression directly, without a priori assuming any particular mathematical form.

There does not yet appear to be an example for which a microstructural model has provided requisite fidelity or generality when a continuum model has somehow failed. We can, however, anticipate such a description becoming more valuable as phenomena such as flow-mediated lysis (e.g., Abkarian et al. 2008) are investigated in greater detail. Interestingly, Reasor et al. (2012) suggested that a coarse-grained microstructural model can also be more efficient.

4. SIMULATION CHALLENGES

Even for the simplest constitutive model, a system of flowing and interacting blood cells presents several simulation challenges. Perhaps most obvious are the large deformations of red blood cells that must be resolved. Fortunately, the linear resolving capabilities of numerical schemes can be assessed through a priori analysis of the methods and a posterior examination of solution spectra, although this is rarely reported for cells. The resolution of nonlinear systems is more difficult to assess. Simulations of flow turbulence, for which nonlinearity also leads to a range of scales, often seem to be more critically evaluated in this regard. The nonlinearity of even the simplest membrane constitutive models is far more complex than that of the Navier-Stokes equations, but likewise generates a challenging range of scales to resolve. Mesh-refinement studies are generally good practice and are probably essential in many cases.

Another challenge is the near incompressibility of the membrane, which introduces a numerical stiffness and thus a significant time-step restriction for explicit time integration. If the fast compressional timescales of the membrane are irrelevant to a particular application, which is usually the case (although perhaps not for cell lysis), then implicit time advancement can damp spurious fast modes without negative consequences. Such methods are challenging but have been implemented for blood cells (Dimitrakopoulos 2007) and similarly complex vesicles (Veerapaneni et al. 2011). A simpler but somewhat ad hoc approach is to select a dilation modulus that nearly preserves the area (Pozrikidis 2005) but is not so time-step restrictive as a physically realistic modulus. This is then a model parameter, which should be verified to not affect results of interest. A third option is to model near incompressibility with an incompressibility constraint, enforced via a Lagrange multiplier, serving the same role as pressure in incompressible flow. Although this approach avoids the time-step restriction, it does introduce a global system to be solved on each cell surface (Veerapaneni et al. 2011). The relative merits of these approaches will generally depend on other features of the overall algorithm and the application needs.

The cell volume also should be fixed, although it will generally drift owing to numerical errors. However, as a well-resolved low-order moment of the cell shape, volume drift is generally small. Volume errors as low as 0.5% for significant deformation have been reported in simulations with modest resolution (Zhao et al. 2010). It is thus easily corrected by moving the membrane in its local normal direction, which might seem ad hoc but is tantamount to a numerically enforced variational constraint (Freund 2007).

Another challenge is the close interactions between cells. In some species, red blood cells can transiently form aggregates, which necessitates the modeling of molecular forces (Popel & Johnson 2005), but even in conditions for which aggregates do not form, cells will come close to each other and vessel walls. For ideally smooth surfaces, lubrication mechanisms in the thin layers of plasma that separate them would preclude contact, and we generally anticipate high-numerical-resolution requirements to resolve these. The reality of interacting cells is of course much more complex. Their glycocalyx coating (Section 3.1), thermal fluctuations of the membrane (Section 2), and macromolecules (e.g., fibrinogen) in blood plasma (**Figure 2*c***) potentially all affect dynamics near contact. Representing molecular forces associated with these features is probably necessary to faithfully represent close interactions in detail, and it is unclear if there are sufficient cell-surface physiologic data to do this precisely in all cases.

In some cases, computational efficiency can be particularly important. The flow of multicell systems can be chaotic, demanding long run times to converge statistics of interest. Similarly, the microvasculature and many engineered devices have fundamentally complex geometry (e.g., **Figure 1*c***). As for any type of simulation, representing this adds cost and can present additional challenges.

A general solver for cellular blood flow needs to address all these challenges, and most problems of interest involve at least some of them. Fortunately, there are several of methods available for both the fluid and solid mechanics, each with certain benefits and drawbacks. Given the range of applications involving blood flow, it is unlikely that any approach will be universally superior. The following section summarizes options for representing the solid mechanics of the cell membrane and addresses its resolution needs. That is followed by a detailed discussion of options for coupling with a flow solver.

5. MEMBRANE DISCRETIZATION

5.1. Issues and Options

In the absence of significant inertia (see Section 2), the membrane is simply advected:

$$\frac{d\vec{\mathbf{x}}}{dt} = \vec{\mathbf{u}}(\vec{\mathbf{f}}(\vec{\mathbf{x}})). \tag{8}$$

The list of surface points $\vec{\mathbf{x}}$ represents the cell surface as a structured mesh, an unstructured mesh, or the collocation points of underlying basis functions. These positions are time integrated according to Equation 8 by an appropriate algorithm. The flow solver provides their corresponding velocities $\vec{\mathbf{u}}$, which depend on the tractions $\vec{\mathbf{f}}$ exerted by the cells upon the fluid. These tractions in turn depend on the deformation of the cells as embodied in $\vec{\mathbf{x}}$. Thus the principal chore of the membrane discretization is to evaluate the constitutive model that determines $\vec{\mathbf{f}}(\vec{\mathbf{x}})$. For simplicity, I neglect membrane viscosity in this discussion but revisit it again in Section 7.2.

Finite elements, with their geometric flexibility and provable properties based on Galerkin projections, are a common choice to discretize the solid mechanics of the membrane (Doddi & Bagchi 2009, MacMeccan et al. 2009). The sphere-like geometry of the cells also facilitates spectral description with spherical harmonics, which offers excellent resolution and convergence (Veerapaneni et al. 2011, Zhao et al. 2010, Zick & Homsy 1982). Spectral-element methods, which are finite-element methods crafted with orthogonal basis functions, offer both convergence and geometric flexibility (Dimitrakopoulos 2007, Muldowney & Higdon 1995) and have been used for detailed simulations of individual blood cells (Dodson & Dimitrakopoulos 2012). Particle representations of the cell membranes, typically based on cell microstructure (Fedosov et al. 2012,

Pivkin & Karniadakis 2008; see Section 3.4.2), provide a unified fluid-solid algorithm with certain advantages (see Section 6.5).

The accuracy of these different discretizations deserves comment. For the smooth cell shapes, well-crafted finite-element methods converge with decreasing element size (h convergence), which is usually quantified with the polynomial order of the element basis functions. Spectral elements share this convergence but also have superalgebraic convergence with polynomial-order refinement (p convergence). Global spectral methods obtain this superalgebraic convergence as well. However, the real utility of convergence depends on the accuracy goals of a simulation.

Dealiasing: a numerical procedure for removing aliasing error

Aliasing: the spurious appearance at resolved scales of the unresolvable scales created by nonlinearity

Very high accuracy might be required for some idealized problems, in which case faster convergence can significantly reduce the cost. These might include establishing an extremely accurate numerical solution that can be used in effect as an exact solution (e.g., Zick & Homsy 1982). However, for blood cells, the uncertainty of the geometry and constitutive models in some cases can obviate the utility of such accuracy. The convergence of a method (its order) is less relevant in this case; accuracy for finite resolution is more important because it reflects how efficiently each numerically represented degree of freedom is used. Mesh independence for important observables can be achieved without a converged pointwise solution, as is often the case in the simulation of chaotic systems. Global spectral methods represent the underlying basis functions exactly, so their resolution can be considered perfect: Every mesh point is used with full fidelity to represent the cell shape. Despite their convergence characteristics, finite- and spectral-element methods do not share this property as the low degree of interelement continuity reduces accuracy for short-length-scale features. Specifically, derivatives are exact for represented modes with global spectral methods but not for others.

Resolution can be quantified via the spectral properties of the discretization, comparing the effective wave number implied by a numerical approximation of, for example, a derivative with the exact wave number (Moin 2010). Effective wave numbers are exact for spectral methods, but even spectral-element methods show significant deviations (Kwok et al. 2001). These notions are central to the simulation of turbulence (Moin & Mahesh 1998), which at present has no hope of convergence to a unique numerical solution. It is the resolution of spectral methods, rather than their convergence, that enabled the first realistic simulations of turbulence.

Order and convergence of a method speak only to linear operations such as differentiation. This is important, but it is not the only source of error. Nonlinearity can transfer energy to scales that are not resolved, although this energy does not disappear as it should to be consistent with the selected resolution. Instead, it is erroneously aliased to resolved scales. This degrades the solution and, perhaps more importantly, also provides a feedback mechanism for possible instability. Because a global spectral discretization provides an exact interpolation to finer meshes, it facilitates a dealiasing procedure commonly used for turbulence (Canuto et al. 1987, Kravchenko & Moin 1997). Evaluated on a finer mesh, the aliased energy can be explicitly filtered in a way that is compatible with the user-selected resolution. In contrast to the incompressible Navier-Stokes equations, dealiasing the nonlinear operations in the cell system is only approximate. Even so, it provides stability without filtering or dissipation (Veerapaneni et al. 2011, Zhao et al. 2010), either of which would degrade the solution fidelity. Thus resolution can be selected based on accuracy rather than stability criteria. Simply carrying more mesh points (or basis functions) is another way to accomplish the same objectives, but at greater cost, especially when one considers the time-step restriction for explicit time advancement. Numerical dissipation or filters sacrifice resolution to counter aliasing errors and stabilize methods.

An elastic shell discretization imposes a time-step restriction for explicit time integration of Equation 8. The details depend of course on the specific formulation, although some general conclusions are possible. The spectral radius based on the elasticity would suggest that

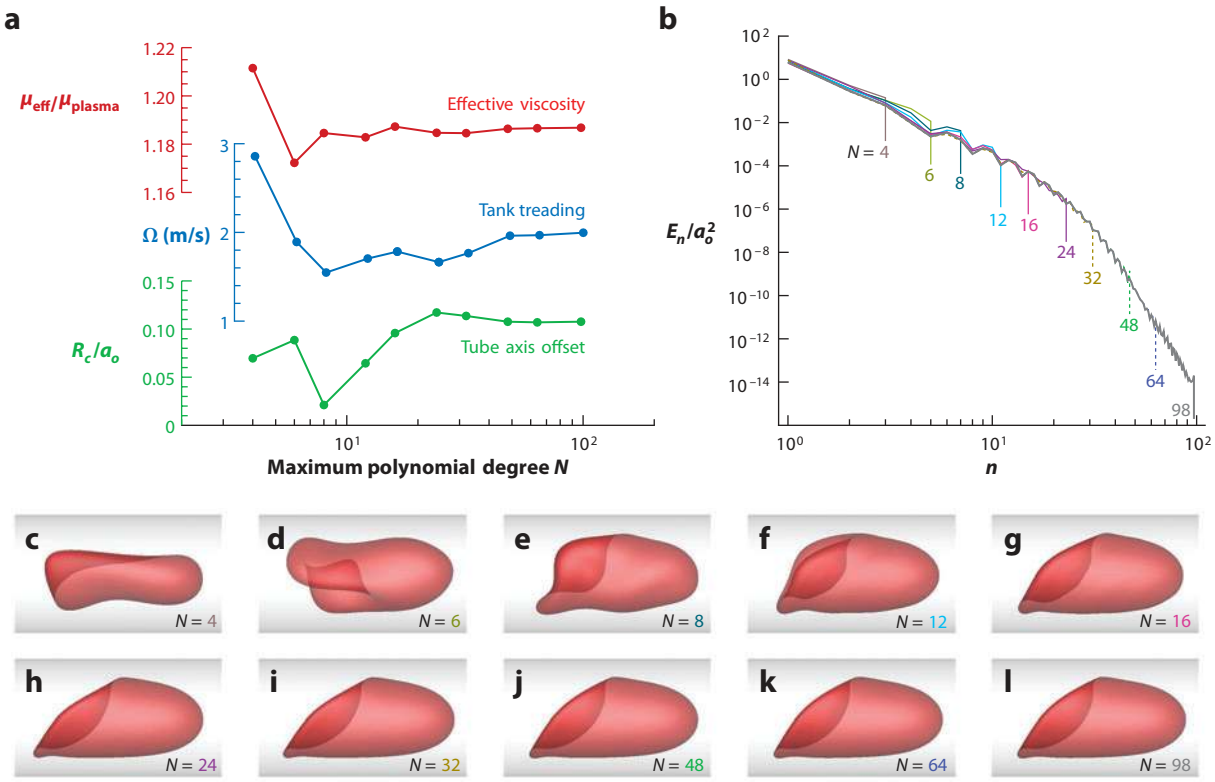

Figure 4

A demonstration of resolution needs showing the refinement of maximum spherical harmonic degree N for a single red blood cell in a diameter $D = 7.05$-μm tube. (*a*) The convergence of effective viscosity μ_{eff}, tank-treading rate (Freund & Orescanin 2011), and radial axis offset. (*b*) Deformation spectra $E_n = \sum_{m=1}^{n}(a_{nm}^2 + b_{nm}^2)$, where a_{nm} and b_{nm} are coefficients of the spherical harmonic expansion (see Freund & Orescanin 2011). (*c–l*) Visualizations for resolutions as labeled.

$\Delta t_{\max} \sim \Delta x^2/E_{d,s}$ for the dilatational or shear resistance and $\Delta t_{\max} \sim \Delta x^4/E_b$ for the bending resistance, although the viscosity of the coupled flow will counter this. For red blood cells, empirical results for a particular boundary integral scheme show (Zhao et al. 2010)

$$\Delta t < \min\left(\frac{2.5\Delta x^{1.2}}{E_d}, \frac{0.19\Delta x^{3.2}}{E_b}\right). \tag{9}$$

In this case, for an E_d selected to preserve the area within a few percent, it was found that the E_d component dictated the time-step restriction for practical resolutions.

5.2. Resolution Needs: A Specific Example

Figure 4 shows a demonstration of the resolution needs for a single red blood cell flowing in a streamwise-periodic tube of diameter $D = 2.5a_o = 7.05$ μm, where a_o is the radius of a sphere matching the cell volume. The tube length is $L = 4.3a_o = 12.2$ μm, so the mean volume fraction of red blood cells (the hematocrit) is $H_c = 0.2$, a number typical for microcirculatory flows. The mean flow velocity is $U = 2.68$ mm/s for a pseudoshear rate $U/D = 380\ \text{s}^{-1}$, which is relatively high physiologically. The cell was initialized off center as a sphere and ended up flowing steadily

Hematocrit: the volume fraction of blood cells

off the tube axis, as has been observed in experiments (Abkarian et al. 2008). Common values of E_s, E_d, and E_b are used (Pozrikidis 2005), with $\mu_{\text{cytosol}} = 5\mu_{\text{plasma}}$ and without membrane viscosity. A spherical reference configuration was selected to remove a small unsteadiness associated with the membrane tank-treading motion for a biconcave reference configuration.

The spherical harmonic basis functions used here are particularly useful for assessing resolution needs. Dealiasing afforded by this description allows us to consider maximum polynomial order N spanning from obviously under-resolved $N = 4$ up to $N = 98$. Each coordinate direction has N^2 degrees of freedom for the cell shape $\vec{\mathbf{x}}$. Cases with $N \leq 16$ used degrees through $M = 48$ for nonlinear operations and quadratures; cases with $N = 24$ to 48 used $M = 2N$; the case $N = 64$ used $M = 128$; and the case with $N = 98$ used $M = 100$. In all cases, the cylindrical wall was discretized with a regular triangular mesh of 9,696 elements.

Figure 4*a* shows the convergence with increasing N of the effective viscosity μ_{eff}, a tank-treading rate Ω (Freund & Orescanin 2011), and the radial centroid location of the cell. Even the poorly resolved $N = 4$ case provides a reasonable measure of the effective viscosity, reflecting the general shape insensitivity of Stokes flow. A similar insensitivity was seen by Pan et al. (2011) for an extremely coarse-grained representation using a dissipative particle dynamics (DPD) model (see Section 6.5). Other observables require higher resolution. The tank-treading metric Ω has $\sim$50% errors for the lowest resolution. The sensitivity of Ω to resolution can be anticipated from the visualizations in **Figure 4*c–l***, which suggest that $N \gtrsim 12$ is needed to remove obvious low-resolution artifacts. Deformation spectra (**Figure 4*b***) show that E_n is well represented through five decades of decay for $N = 12$, which provides a resolution guideline. This figure also shows that even in the obviously under-resolved cases, the low-order basis functions still provide a reasonable model for those in the highly resolved cases. For $N \gtrsim 16$, all the spectra lay atop one another.

6. FLOW SIMULATION METHODS

6.1. Overview

There are myriad methods for discretizing the flow equations. Eulerian finite-difference and finite-volume methods, the traditional workhorses of computational fluid dynamics, are complemented by the semi-Lagrangian lattice Boltzmann method, which has some advantageous properties for incorporating the cells. The low Reynolds numbers also enable dissipative particle schemes. If inertia is to be completely neglected (Section 2), then the linearity of the flow equations and the availability of Green's functions can be used in boundary integral discretization. Regardless of the method selected, integrating the flow solver with the solid mechanics discretization requires special attention, as it risks the introduction of significant error and potential instability. However, in the inertia-free limit, especially if membrane viscosity is neglected, the combined dynamics in Equation 8 can be broken into a series of one-way coupled steps, $\vec{\mathbf{x}} \rightarrow \vec{\mathbf{f}} \rightarrow \vec{\mathbf{u}} \rightarrow \partial_t \vec{\mathbf{x}}$, which simplifies the formulation. This section reviews various methods for computing velocities $\vec{\mathbf{u}}$ given $\vec{\mathbf{f}}$.

6.2. Boundary Integral Methods

The mathematical foundation of Odqvist (1930), as summarized and extended by Ladyzhenskaya (1969), was crafted into an integral-based numerical method by Youngren & Acrivos (1975), the generalization of which by Rallison & Acrivos (1978) for finite-viscosity drops is particularly relevant for cells. The overall formulation, emphasizing numerical applications, has been summarized in detail by Kim & Karrila (1991) and Pozrikidis (1992). The linear viscous flow equations, with

imposed mean flow velocity $\mathbf{U}^\infty$ and $\mu_{\text{cytosol}} = \lambda\mu_{\text{plasma}}$, are equivalent to

$$u_j(\mathbf{x}) = \frac{2}{1+\lambda}U_j^\infty - \frac{1}{8\pi\mu(\lambda+1)}\int f_i(\mathbf{y})G_{ij}(\mathbf{y},\mathbf{x})dS(\mathbf{y}) + \frac{1}{8\pi}\frac{1-\lambda}{1+\lambda}\int^{\mathcal{PV}} u_i(\mathbf{y})T_{ijk}(\mathbf{y},\mathbf{x})n_k(\mathbf{y})dS(\mathbf{y}), \tag{10}$$

where for $r_i = x_i - y_i$, the Green's functions

$$G_{ij} = \frac{\delta_{ij}}{r} + \frac{r_i r_j}{r^3} \quad \text{and} \quad T_{ijk} = -6\frac{r_i r_j r_k}{r^5} \tag{11}$$

yield velocity $\mathbf{u}$ and stress σ solutions

$$\mathbf{u}_i = \frac{1}{8\pi\mu}G_{ij}g_j \quad \text{and} \quad \sigma_{ij} = \frac{1}{8\pi}T_{ijk}g_k \tag{12}$$

of the viscous flow equations for a singular source

$$-\nabla p + \mu\nabla^2\mathbf{u} = \mathbf{g}\delta(\mathbf{x}-\mathbf{y}) \quad \nabla\cdot\mathbf{u} = 0. \tag{13}$$

Quadrature of Equation 10 with N_p discrete points leads to a linear system

$$\vec{\mathbf{u}} = \frac{2}{1+\lambda}\mathbf{U}^\infty + \frac{1}{1+\lambda}A\vec{\mathbf{f}} + \frac{1-\lambda}{1+\lambda}B\vec{\mathbf{u}}, \tag{14}$$

where A and B are $N_p \times N_p$ matrices. Given $\vec{\mathbf{f}}$, the solution $\vec{\mathbf{u}}$ is required by Equation 8.

A benefit of this approach is that only surfaces are discretized (**Figure 5*a***), so the possibly narrow space between cells does not need to be resolved. The integrands of Equation 10 do become sharper as cells become close, but this requires only surface refinement. This method also avoids errors associated with interpolating velocities to the cell surfaces from a flow-solution mesh as is required in some formulations (see Section 6.3). A disadvantage is that it is strictly limited to linear viscous flow. It is also somewhat cumbersome compared to standard flow solvers in terms of specifying boundary conditions. It can require auxiliary algorithms, for example, to enforce a constant velocity condition.

In crafting the quadratures, care must be taken regarding the singular kernels (**Figure 5*b***). L'Hôpital's rule is sufficient for some terms, but others are usually handled by subtracting out a local function with the same singular behavior, leaving only a smooth function to be integrated over the cell surface. This singular term is then evaluated independently with sufficient accuracy and added back in. In two dimensions, this can be done analytically; however, it seems that in three dimensions, it requires quadrature on a local fine mesh (Muldowney & Higdon 1995, Zhao et al. 2010). Veerapaneni et al. (2011) provided a thorough discussion of these issues.

Treating the singular points in this way can constitute a significant fraction of the overall computational expense; however, the same machinery can also increase accuracy for close interactions, when the integrands display nearly singular behavior (**Figure 5*c***). This imbues the method with a secondary property, the value of which does not seem to be widely recognized: Close interactions between cells can be accurately represented. A direct approach would require increasing the resolution of the entire surface mesh. This nearly singular formulation instead takes advantage of the relative smoothness of the cell shape compared to the integrand.

The details of the development of Equation 14 from Equation 10 depend on the various choices of the discretization, including the singular-point treatment. In most cases, however, Equation 14 is not formed explicitly to avoid costly dense-matrix operations. Even in the uniform-viscosity case, where $\lambda = 1$, the costly $O(N_p^2)$ dense matrix–vector multiplication $A\vec{\mathbf{f}}$ would outweigh the benefits of this approach for even modest-sized systems. When $\lambda \neq 1$ (Equation 14), the dense-matrix solution for $\vec{\mathbf{u}}$ is even more expensive. Fortunately, there are ways to solve Equation 14

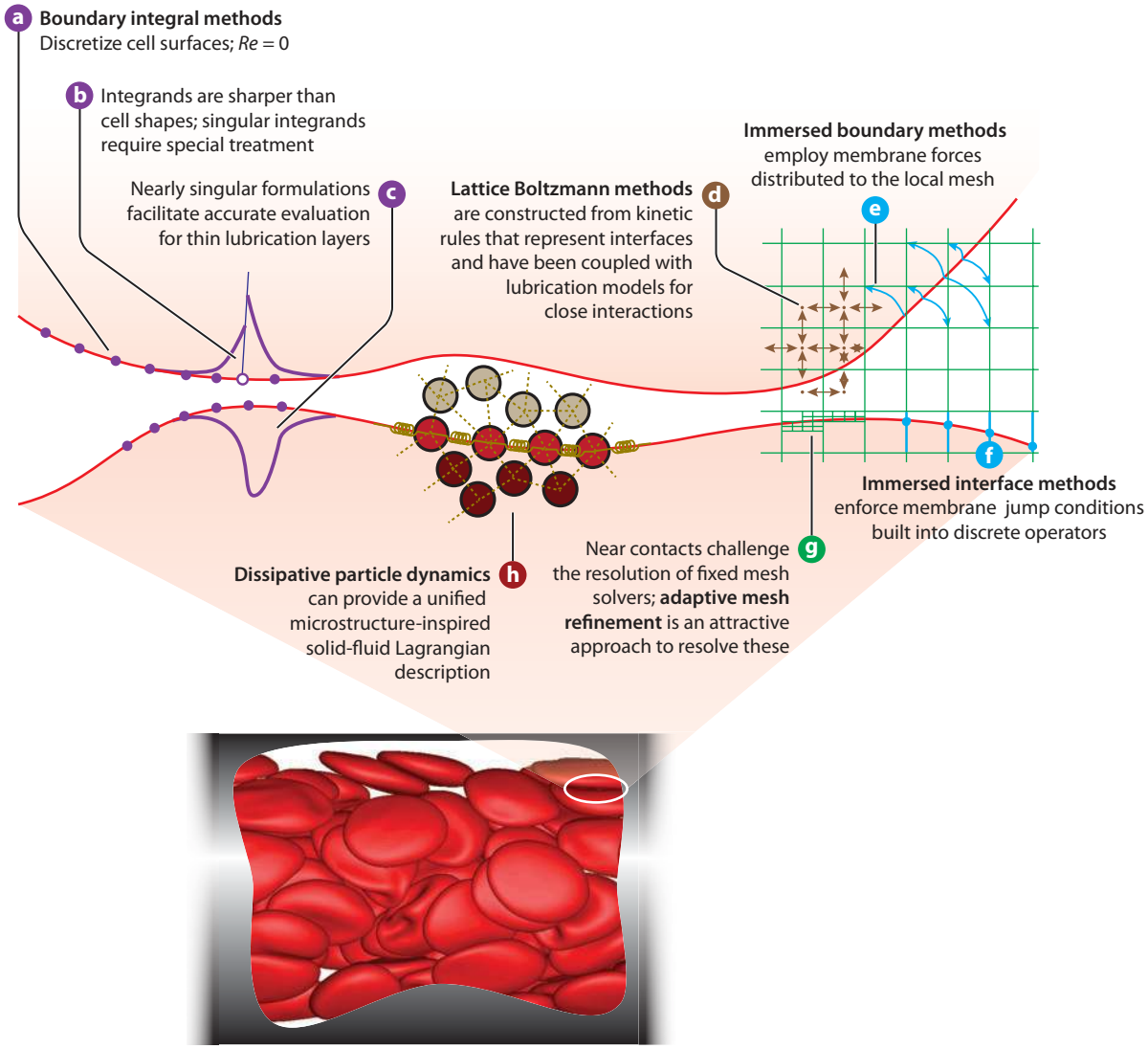

Figure 5

Various aspects of available schemes for solving the dynamics of the cell membranes, represented here as red curves or surfaces.

accurately with $O(N_p)$ or $O(N_p \log N_p)$ operations. Matrices A and B in Equation 14 are dense because of the slow spatial decay of the Green's functions (Equation 11). The two most widely used methods utilize the Green's function structure for fast approximate evaluation of the matrix-vector operations in Equation 14. Within an iterative scheme, this also facilitates fast solution for $\vec{\mathbf{u}}$. Particle-mesh and multipole methods are discussed in the following two subsections.

6.2.1. Particle-mesh methods. This approach starts with a decomposition of the Green's functions into short-range singular and smooth parts, such that $G_{ij} = G^{\mathrm{sr}}_{ij} + G^{\mathrm{sm}}_{ij}$, which was first applied to the Stokes Green's function by Hashimoto (1959). Both G^{sr} and T^{sr} have a

Gaussian decay, so unlike the full G and T, these can be accurately truncated to form sparse $O(N)$ matrix–vector products: $A^{sr}\vec{\mathbf{f}}$ and $B^{sr}\vec{u}$. The smoothness of the remaining long-range interactions in $A^{sm} = A - A^{sr}$ and $B^{sm} = B - B^{sr}$ facilitates a Fourier description that decays rapidly in wave-number space. It can also be interpolated to a mesh and evaluated with fast Fourier transforms (FFTs), reducing the expense to $O(N_p \log N_p)$. These are known as particle-mesh-Ewald (PME) (Darden et al. 1993) or particle-particle-particle-mesh (P^3M) (Hockney & Eastwood 1988) methods. In their formulation, there are many opportunities to reduce overall error by canceling those of different suboperations. This approach seems to have been first applied to Stokes flow systems by Higdon and coworkers (Guckel 1997, Metsi 2000). It has been used in fast Stokesian dynamics (Sierou & Brady 2001) and was developed into its apparent state-of-the-art form for more general suspensions by Saintillan et al. (2005). It was first used for blood cells in two and three dimensions by Freund (2007) and Zhao et al. (2010), respectively.

In addition to being $O(N_p \log N_p)$ (assuming as usual that an FFT is used), these PME/P^3M methods have a small operation-count coefficient, making them a common choice for accurate evaluation of modest-sized N-body sums. A notable disadvantage is that the nonlocality of the FFT hinders implementation and efficient scaling on parallel computers. Also, because these algorithms involve balancing the errors of so many subcomponents, selection of the numerical discretization parameters (e.g., the short-range cutoff, the FFT-mesh size, the splitting parameters of the Green's functions, and the B-spline interpolation order) can be significantly more involved than standard flow solvers (Hockney & Eastwood 1988). Periodic boundary conditions are most natural for FFTs, but there are straightforward ways at a modest additional cost to implement free-space boundary conditions (Freund 2002, Hockney & Eastwood 1988, Pollock & Glosli 1996).

6.2.2. Fast multipole methods. A second approach to fast evaluation of the matrix-vector products in Equation 14 employs multipole expansions of the Green's functions, extending the method first developed by Greengard & Rokhlin (1987). These expansions provide means of grouping long-range interactions, with expansion coefficients that can be developed hierarchically in a way that leads most directly to an $O(N_p \log N_p)$ algorithm. Additional expansions can yield $O(N_p)$. This approach appears to have been first formulated for Stokes flow by Greengard & Rokhlin (1987), developed and used by Sangania & Mo (1996) for particles and by Zinchenko & Davis (2000) for deformable drops, and applied to massive blood cell simulations by Rahimian et al. (2010), seemingly just to demonstrate its parallel scaling. It has also recently been used in two dimensions for a vesicle model of red blood cells by Selmi et al. (2011).

Fast multipole methods are elegant but are not as commonly used for problems of current practical size. Despite the $O(N)$ scaling, the coefficient is very large, $\sim 10^3 p^4$ in the original formulation (Greengard 1988), where p is the order of the multipole expansion. It has been suggested that electrostatics problems with even huge numbers of points will be more efficiently handled with PME/P^3M schemes (Pollock & Glosli 1996). However, different expansions and better adaptivity have reduced operation counts significantly to $150p + 5p^2$ or $47p^{3/2} + 2p^2 + 40p^{1/2}$ (Cheng et al. 1999). It seems that about 1,800 floating point operations per singularity are required for 10^{-4} relative errors in electrostatic systems (Cheng et al. 1999), and it is expected that the Stokes singularities will follow approximately this same scaling (Tornberg & Greengard 2008).

An attractive feature of fast multipole methods is that long-range interactions are grouped, so unlike FFT-based methods, parallel implementation can be made efficient with judicious data management. Because empty regions demand no computational effort, these methods are also naturally adaptive. In contrast to PME/P^3M, the natural formulation is free space, but periodic conditions are possible (Greengard & Rokhlin 1987, Lambert et al. 1996).

6.3. Mesh-Based Methods

The most common approach of computational fluid dynamics is the discretization of the Eulerian flow equations on a mesh that fills the flow region. With this approach, it is straightforward to develop methods that scale linearly (or close to linearly) with the problem size. It is also easy to include finite inertia, which does not seem possible with boundary integrals. However, other challenges are introduced. Foremost of these are the complex and changing cell shapes, which at present remain beyond the capabilities of efficient dynamic mesh motion algorithms. The degree of deformation and changing relative positions of the cells would necessitate substantial and frequent mesh regeneration, which is computationally expensive. To avoid the meshing challenge, the flow equations are typically solved on a fixed mesh that does not conform to the cell shapes. This provides the accuracy and speed of fixed-mesh algorithms, although it requires additional formulations to couple the fluid flow with its moving elastic boundaries. The requisite interpolations introduce additional approximations, although errors do not seem prohibitive. The insensitivity of Stokes flow to fine geometric details is probably helpful in maintaining accuracy despite the nonconforming meshes.

A particular challenge for a fixed mesh is representing close hydrodynamic interactions between cells, whether this is modeled as true solid-body contact, near contact with lubrication layers, steric repulsion, or some other molecular interaction. Uniform meshes that are sufficiently fine for accurate computation of the flow in spaces between cells would lead to huge numbers of overall mesh points. Forces that arise in the lubrication limit are strongly sensitive to fluid gap width, which might demand particularly accurate representation in some cases. It is intriguing that velocity profiles are quadratic in the lubrication limit, so derivatives in principle can be exactly computed with second-order methods, although it is unclear if any of the present schemes have benefited from this.

For rigid particles, lubrication forces are particularly strong and in some cases can be regarded as pairwise interactions, which is the foundation of the Stokesian dynamics description of suspension hydrodynamics (Brady & Bossis 1988). In the rigid-particle limit, these lubrication layers can dominate interactions (Nunan & Keller 1984). They can also introduce long timescales (Melrose & Ball 1995). Corrections for fixed-mesh schemes that approximate lubrication forces have been developed based on a leading-order singularity of the resistance matrix for simple particles (Nguyen & Ladd 2002) or an approximation of that based on the local curvature (Ding & Aidun 2003). Both are reasonable regularizations, facilitated for rigid particles by the fact that these forces dominate close interactions, although a full analysis for flexible membranes is probably warranted. The requisite fidelity for representing lubrication forces in flowing blood has not been thoroughly studied and is probably dependent on the application. Given the high deformabilty of cells, we can speculate that increasing lubrication pressures will more easily deform the cells than squeeze out the thin lubrication layers.

Both finite-difference and lattice-Boltzmann discretizations have been used successfully with nonconforming meshes (see the sidebar, Stokesian Dynamics). These are discussed in the following subsections.

6.3.1. Finite-difference methods. There is a wealth of finite-difference methods for solving the flow equations in a meshed volume, although most have been designed for moderate or high Reynolds numbers, so application to cellular blood flow warrants some consideration. A general discretization of the incompressible flow equations,

$$\frac{\partial \mathbf{u}}{\partial t} + \mathbf{u} \cdot \nabla \mathbf{u} = -\nabla p + \frac{1}{Re} \nabla^2 \mathbf{u} \quad \nabla \cdot \mathbf{u} = 0, \tag{15}$$

STOKESIAN DYNAMICS

Stokesian dynamics provides a numerical description of suspension hydrodynamics (Brady & Bossis 1988, Durlofsky et al. 1987). The goal, which is shared by cell simulations, is to relate forces on particles $\vec{\mathbf{f}}$ to their velocities $\vec{\mathbf{u}}$. The linearity of the Stokes limit guarantees the existence of a mobility matrix $\mathcal{M}$ such that $\vec{\mathbf{u}} = \mathcal{M}\vec{\mathbf{f}}$ or, alternatively, a resistance matrix, $\mathcal{R} = \mathcal{M}^{-1}$, such that $\vec{\mathbf{f}} = \mathcal{R}\vec{\mathbf{u}}$. The success of this method depends on the inclusion of both long-range and lubrication interactions in $\mathcal{M}$. Building the long-range $\mathcal{M}^f$ from pairwise interactions provides a fairly accurate approximation, and these are readily available in mobility form for simple shapes such as spheres. The inverse $\mathcal{R}^f$ thus represents many-body, long-range interactions. To this are added lubrication interactions $\mathcal{R}^l$, which are effectively pairwise with analytic lubrication-limit resistance forms available. With $\mathcal{R} = \mathcal{R}^f + \mathcal{R}^l$, the full system can be inverted to provide particle motion via $\mathcal{M}$. Although the same long-range and lubrication interactions are involved in the cell system, the utility of this approach relies on the availability of accurate analytical formulas, which exist for simple shapes like spheres but not for the general shapes of cells. However, because it is grounded in analytically tractable limits, the Stokesian dynamics description can illuminate the mechanisms in blood. Furthermore, applying some of the same principles could facilitate the acceleration of numerical methods or provide a framework for the multiscale modeling of cellular systems.

from time level n to $n+1$ can be written as

$$\begin{bmatrix} A & G \\ D & 0 \end{bmatrix} \begin{bmatrix} \mathbf{u}^{n+1} \\ p \end{bmatrix} = \begin{bmatrix} r^n \\ 0 \end{bmatrix}_{\text{explicit r.h.s.}} + \begin{bmatrix} b_u \\ b_p \end{bmatrix}_{\text{boundary cond.}}, \tag{16}$$

where p enforces incompressibility, D and G are discrete divergence and gradient operators, and A and r^n depend on the time-advancement algorithm. For time-implicit viscous terms and time-explicit convective terms, $A = I/\delta t + L/Re$, with L representing the stress divergence operator. Fractional-step methods (Chang et al. 2002, Kim & Moin 1985), which have been so widely used for flow simulations, are based on an exact rearrangement of Equation 16,

$$\begin{bmatrix} A & 0 \\ D & -DA^{-1}G \end{bmatrix} \begin{bmatrix} I & A^{-1}G \\ 0 & I \end{bmatrix} \begin{bmatrix} \mathbf{u}^{n+1} \\ q \end{bmatrix} = \begin{bmatrix} r^n \\ 0 \end{bmatrix}_{\text{explicit r.h.s.}} + \begin{bmatrix} b_u \\ b_p \end{bmatrix}_{\text{boundary cond.}}, \tag{17}$$

which is often solved in a three-step approach assuming $A^{-1} \approx I\delta t$:

$$Aw = r^n + b_u \quad \text{(solve for intermediate velocity } w\text{)}, \tag{18}$$

$$DGp = Dw \quad \text{(solve for pressure with } b_p\text{)}, \tag{19}$$

$$u^{n+1} = w - Gp \quad \text{(project out compression)}. \tag{20}$$

For $Re \to 0$, r^n is negligible, and Equation 20 guarantees discrete incompressibility $Du^{n+1} = 0$, but solving in this limit can introduce a significant splitting error into the momentum balance because $A^{-1} \not\approx I\delta t$. Fractional-step approaches have been used for $Re = 0.01$ (Doddi & Bagchi 2009, Yazdani & Bagchi 2011), but the consequences of this splitting error do not seem to have been investigated. An exact splitting, based on a discrete curl operator and a corresponding discrete stream function, would seem to eliminate this (Chang et al. 2002).

To include cells, one must represent the force exerted on the fluid by the cell membrane. Immersed boundary methods distribute this singular force to nearby points using a discrete analog

of the Dirac δ-function (Mittal & Iaccarino 2005) (**Figure 5*e***). Because there are not boundary layers in the viscous flow limit, this smearing procedure is relatively benign. However, faithful representation of close interactions is now also limited by the length scale of this distributed force.

Sharper interfaces can be represented by immersed interface methods (LeVeque & Li 2003), which modify the discrete operators to include interface jump conditions (**Figure 5*f***). This is intricate even for rigid objects (Xu 2008). For the viscosity discontinuity of red blood cells, there is no local representation of these jump conditions, although a nonlocal condition can be formulated as a boundary integral (Biros et al. 2003), or the jump conditions can be incorporated as an unknown into an overall iterative solver (Li et al. 2007). The sharp representation afforded by this method is attractive, but it does not appear that immersed interface methods have yet been used for flowing blood cells. Although relatively sharp, they would not, however, entirely solve the problem of close approach, as it remains unclear how cell interactions of less than a mesh spacing could be represented. It might be possible to include lubrication models along with the jump conditions in modifying the discrete operators.

Adaptive mesh refinement, which would cluster points adjacent to the membranes (e.g., Vigmostad et al. 2010), could alleviate this, but it also does not seem to have been applied to cellular blood flow. However, we can anticipate future efforts in this direction (**Figure 5*g***).

6.3.2. Lattice-Boltzmann methods. Similar to finite-difference methods, lattice-Boltzmann methods use a fixed volume-filling mesh (**Figure 5*d***). However, they are founded on a description that yields the mechanics of the Navier-Stokes equation in a statistical limit (Aidun & Clausen 2010, Higuera & Jiménez 1989). The resulting scheme is simple to implement even in complex geometries, localized in a manner compatible with efficient implementation on modern parallel computers, and requires a small operation count. Galilean invariance is only approximate, although this does not seem to be restrictive. In their basic form, these methods are second-order accurate and share a similar dispersion error with low-order finite-difference schemes (Xu & Sagaut 2011). Given the recent thorough review of these methods (Aidun & Clausen 2010), I only summarize some basic considerations. The lattice-Boltzmann method has reproduced key features of blood rheology (MacMeccan et al. 2009, Reasor et al. 2012) and facilitated the qualitative investigation of cellular interactions (Sun & Munn 2008).

One consideration, of potential importance for cellular blood flow, is that the $Re \to 0$ limit is challenging. The statistical description of the flow equations is intertwined with a microscopic viscous relaxation timescale, with the result that the computational expense increases as $1/Re$ for $Re \to 0$. However, it is possible to achieve $Re < 1$ and thus study flow in viscously dominated regimes (Reasor et al. 2012). Care is needed to avoid spurious finite-inertia effects, just as the complete absence of inertia must be recognized in interpreting boundary integral results, but this is not a fundamental limitation.

The most direct kinetic bounce-back method for coupling the moving boundary of the cells to the regular mesh yields a first-order approximation. Means of improving the accuracy, via interpolation or extrapolation or by adjusting the collision operators of the underlying statistical description, can improve accuracy at the cost of simplicity (Aidun & Clausen 2010).

6.4. Hybrid Integral-Mesh Methods

Kumar & Graham (2012a) have developed a hybrid method that shares features of both boundary integral and mesh-based methods. In essence, a boundary integral equation is employed for a short-range component of the interaction between two singular points on cell boundaries, using a

free-space Green's function that is functionally equivalent to the short-range portion of the PME/P^{3}M Green's function. However, the FFT solution is replaced with a mesh-based Stokes flow solution, which includes the smoothed components of the singular forces and any wall boundary conditions. The combined scheme has the benefits of boundary integrals for close interactions coupled with the wall geometry flexibility and boundary condition convenience of mesh-based schemes.

This overall approach fits within the broad scope of P^{3}M methods, which includes non-FFT solutions for the smooth part of the decomposition (Hockney & Eastwood 1988). In general, this does not realize the same error cancellation afforded by the FFT discretization, although the advantage of the explicit representation of complex geometric boundary will potentially outweigh this drawback. Kumar & Graham (2012a) implemented it with a Fourier-Chebyshev flow solver, which provides an accurate baseline and demonstrated their method for several confined-flow geometries. There is perhaps an opportunity for further improvement via optimization of the implied P^{3}M influence function to account for the errors in the mesh solution (Hockney & Eastwood 1988).

6.5. Stochastic Particle Methods

Stochastic particle methods are often based on a dissipative particle dynamics (DPD) method first proposed by Hoogerbrugge & Koelman (1992), in which the system is modeled mesoscopically by particles, motivated by its underlying molecular makeup but each representing large groupings of actual molecules (**Figure 5*b***). Each of these superparticles is simple, without any internal degrees of freedom. They interact via pair potentials designed to represent the material of interest. The chemical character of interactions is heuristically represented by a deterministic interaction $F_{ij}^C(r_{ij})$. This is complemented by dissipative $F_{ij}^D(r_{ij}, u_{ij})$ and random $F_{ij}^R(r_{ij})$ forces, which together maintain a target temperature for the system (Koumoutsakos 2005). This is similar to Brownian dynamics, often used to simulate the long-timescale behavior of polymers, but it includes a detailed balance between particles and thus also can provide a numerical solution of the flow equations.

Unlike continuum-based formulations, the unified discretization of DPD methods naturally couples flow with microscopic structural models. Detailed and coarse-grained spring-based models of red blood cell mechanics have been implemented (Fedosov et al. 2010, 2012, Pivkin & Karniadakis 2008), which have reproduced experimental results. A particular advantage is that membrane viscosity is automatically included, whereas it is challenging to include in most other methods (see Section 7.2). Given the low degree of particle-to-particle continuity, such methods would require larger numbers of particles to accurately represent sharp cell features such as in **Figure 4**, but it is also clear that such resolution is not necessary for many objectives. DPD will potentially be advantageous if thermal fluctuations are important, although it is currently unclear if it has sufficient resolution to represent hydrodynamics on the same ∼200-nm scale of the membrane thermal fluctuations.

Noguchi & Gompper (2005) used a related multiparticle collision dynamics model (Gompper et al. 2008) to simulate blood cells. This is similar to DPD, with the key difference that virtual collisions take place according to a schedule with fixed Δt rather than dynamically. This introduces an additional model parameter but avoids fast timescales associated with the implicit compressibility of DPD. Although there is low fidelity for representing hydrodynamic details, these methods can also be used to study the interesting phenomenology of blood cells. For example, Noguchi & Gompper (2005) show a switch from axisymmetric to nonaxisymmetric behavior for a red blood cell flowing down a narrow tube.

7. ADDITIONAL CHALLENGES

7.1. Stiff or Rigid Particles

The sections above focus on the simulation of red blood cells, particularly on the key challenge of including their high deformabilty. However, rigid particles can provide a model for white blood cells (Krasik et al. 2008), platelets (Mody & King 2008, Zhao et al. 2012), and suspended particles such as magnetic beads (Freund & Shapiro 2012). A rigid model presents an additional challenge.

Including rigid-body motion in boundary integral methods (Equation 10) leads to a singular system. This can be resolved by projecting the six rigid-body velocity eigenvectors out of the linear system in Equation 14, treating them analytically, and then reintroducing them (Kim & Karrila 1991, Pozrikidis 1992). Although tedious, this is compatible with typical algorithms and is fairly easy to test. This same procedure can also accelerate convergence when vesicles contain a high- or low-viscosity fluid, which renders the system nearly singular (Pozrikidis 2001).

For mesh-based solution, rigid particles introduce, in effect, an infinitely fast timescale across the particle dimension, which can restrict the permissible time step. An implicit time advancement seems necessary for particle motions, at least for particles that extend over several mesh cells (Ladd & Verberg 2001).

7.2. Viscoelastic Membranes

As discussed in Section 3.3, the red blood cell membrane is expected to be viscous, and models for this have existed for some time (Evans & Hochmuth 1976a). However, in most simulations, membrane viscosity is neglected. This is in part because the formulation for viscous flow on a time-evolving manifold is intricate, even for a simple Kelvin-Voigt model, which assumes viscous and elastic stresses to be additive (Secomb & Skalak 1982). Recent efforts to recraft traditional formulations (Aris 1962) to facilitate simulation (Arroyo & DeSimone 2009) do not substantially simplify it. However, beyond the additional complexity, the real challenge is that viscoelasticity precipitates the reformulation of the governing equations. It requires that an implicit dependence on $\vec{\mathbf{u}}$ be added to Equation 8, yielding

$$\frac{d\vec{\mathbf{x}}}{dt} = \vec{\mathbf{u}}(\vec{\mathbf{f}}(\vec{\mathbf{x}}, \vec{\mathbf{u}})). \tag{21}$$

A linear implicit system for $\vec{\mathbf{u}}$ already exists in boundary integral formulations (Equation 14), but viscoelasticity is nonlinear owing to geometric factors. Fortunately, viscoelasticity does not seem necessary to reproduce some basic phenomenology of blood flow, such as its effective viscosity in narrow tubes (**Figure 3**), although the bounds of its importance are unclear, as discussed in the context of experimental observations in Section 3.3. Stochastic particle methods (see Section 6.5) include a viscosity much more readily (Fedosov et al. 2010, Noguchi & Gompper 2005) than other formulations, which is one of their key advantages. For these, linear viscosity coefficients can be deduced from the collision model parameters, but a general continuum model for viscous effects has not been formulated. That said, for red blood cells, it is currently unclear if there are sufficient data available to support a more detailed viscosity model.

8. SUMMARY AND OUTLOOK

Above I motivate the cell-scale simulation of flowing blood, summarize its challenges, and present an array of simulation methods that can and have been integrated to meet these challenges. As part of this, experimental data are reviewed to provide a sense of their availability for constitutive modeling and validation. A goal was to emphasize the respective benefits and drawbacks of different

models and numerical methods. I hope this was done in a balanced way, with sufficient emphasis on this important point: The best numerical methods, their needed resolution, and the constitutive models employed will depend on the details and goals of their application.

Sorting out the simulation and modeling needs for different objectives is a near-term goal for work in this area. Some applications will benefit from high convergence order or high resolution, whereas for others, the speed afforded by nominally lower accuracy and coarse graining will be relatively advantageous. For any given objective, the best means are still being worked out for flow-structure coupling, selecting complex and uncertain constitutive models, the near incompressibility of membranes, the mix of relatively rigid and flexible particles, and close interactions and contacts. More detailed experimental data will aid this, especially if they are acquired specifically for flow situations; the uncertainty regarding the applicability of deformations imposed artificially by pipettes, beads, or other means will remain a concern for some time. Microfluidic devices designed to simultaneously create complex flow interactions and measure the resulting cell response with quantitative diagnostics will be invaluable in identifying needs.

In the longer term, methods for large-scale simulations will have to adapt to changing computer platforms. It is anticipated that systems will tend toward greater concurrency and greater heterogeneity, and this will affect algorithm choices. For example, methods that use boundary integrals with FFT-based fast solvers will not scale well, and in these cases, alternatives such as multipole methods or hybrid integral-mesh methods will likely be preferable.

The absolute simulation cost is important and underlies some of the statements made in this review, but I avoid general conclusions in this regard because they are challenging to make precisely. It is easy to state that the simulation with $N = 16$ in **Figure 4** took 10 s per $\Delta t = 30$-μs time step running on two cores of a 2.4-GHz Intel Xeon workstation and that the 90-cell case visualized in **Figure 5** with this same cell resolution and 51,000 wall elements took 200 s per time step on eight cores of the same system, but such statements are of only moderate value. They do not speak to the fidelity achieved for the quantity of interest, do not take into account any serial and parallel code optimizations, and certainly do not assess important but vague factors such as developer and user time. For purposes of this review, general efficiency and accuracy statements are made, but these are not presented on a specific per–floating point operation or similar computational cost basis. All schemes reviewed have satisfied a sufficiency condition in this regard: They have been, or at least could have been, used for fluid mechanics studies of multicell systems using present-day computational resources.

For simulating blood cell fluid mechanics, increasing the physical realism of the models will remain a challenge. Whatever the modeling approach, there will be a need to improve models for the flow-coupled effects of red blood cell aging, lysis, fatigue, disease, ATP metabolism, aggregation, interactions with metastatic cancer cells, and so on. Similarly, a fuller description of the physical environment of blood cells will broaden the potential impact of such simulations in biology and biomedicine. For example, better modeling of the endothelial glycocalyx will facilitate a physically realistic representation of small vessels (Weinbaum et al. 2007). Some of these circumstances might benefit from the application of inverse approaches for calibrating models and for quantifying their inherent uncertainty. Better physical models, perhaps developed in conjunction with simulation, and better numerical implementations are probably more important—and more challenging—than the brute-force representation of larger systems of cells, as continuum models perform well for systems significantly larger than the cell scale.

We can also anticipate ample opportunities for improved models of the collective system in ways that are either illuminating regarding the core mechanisms or beneficial for advancing simulation capabilities. These are likely to be scale-bridging models spanning between relatively large vessels, mid-sized red blood cells, and small platelets or suspended particles or macromolecules. Transport

models, such as the stochastic margination model of Kumar & Graham (2012b), could be coupled with the more detailed models considered in this review to broaden their applicability to larger systems and longer times. Likewise, the short length scales and timescales of binding kinetics, as an example, might be amenable to a Stokesian dynamics description within a more detailed blood cell simulation, which could also provide instantaneous mobilities of the binding components.

Although the simulation techniques and core fluid mechanics are built on rigorous foundations, the simulation of cellular blood should be recognized as applied fluid mechanics. The long-term impact of such simulations will depend on their utility in understanding blood flow and in the design of devices that handle it. Maintaining a focus on biological questions and biomedical needs will be important.

SUMMARY POINTS

1. The cellular detail of blood is an essential feature of its flow mechanics in small configurations. Simulations can reveal phenomena, quantify it, and potentially aid in the design of devices to process blood on the cellular level.
2. Cell-scale blood flow is fundamentally viscous although also significantly nonlinear because of the geometric nonlinearity of the cells and their constitutive models.
3. Sufficient experimental data are available to parameterize both continuum and microstructure constitutive models for red blood cells.
4. Key simulation challenges are (*a*) the flexibility of red blood cells, (*b*) the coupling of the flow dynamics with the elastic deformations of the cells, (*c*) the interaction of the cells at close distances, (*d*) the dilatational stiffness of the cell membrane, and (*e*) the computational expense of solving complex (often chaotic) systems for long times.
5. The linear fluid mechanics allows a boundary integral description, which is particularly advantageous because it (*a*) can resolve close interactions and (*b*) provides direct fluid-structure coupling without additional discrete approximations.
6. Mesh-based methods can draw on the vast set of tools available in computational fluid dynamics. Of these, lattice-Boltzmann methods are particularly (*a*) simple to implement, (*b*) relatively flexible for efficiently representing complex geometries, and (*c*) easily implemented in parallel.
7. Stochastic particle dynamics methods (*a*) provide a unified framework for coupling fluid and solid mechanics; (*b*) fundamentally include thermal fluctuations; and (*c*) naturally include membrane viscosity, which is challenging in many formulations.
8. Different applications will benefit from the advantages of different methods. No single method is expected to be universally advantageous.

FUTURE ISSUES

1. Most constitutive models are based on configurations that do not necessarily provide deformations corresponding to the needs of flow simulation. Codesigned experiments and simulations will focus effort on the fluid mechanical impact of constitutive models and best guide their refinement for predicting flow phenomena with higher accuracy in more extreme flow conditions.

2. The long-term impact of such simulations depends on their utility in blood biophysics and particularly on the design of interventions and biomedical devices that involve cell-scale blood flow.
3. Effective viscosity and similar measurements provide useful baselines but are insensitive to model and numerical errors owing to the general diffusive character of Stokes flow. More detailed applications will need experimental data that are more sensitive to cell properties.
4. Adaptive mesh refinement techniques could significantly increase the efficiency of mesh-based methods, especially flows with close interactions between cells.
5. Multiscale modeling, perhaps informed by detailed simulations of the kind reviewed above, will broaden the range of space and timescales that can be studied.

DISCLOSURE STATEMENT

The author is not aware of any biases that might be perceived as affecting the objectivity of this review.

ACKNOWLEDGMENTS

The author is grateful for helpful comments on a draft of this article from Ms. Natalie Beams. Support from the NSF (CBET 09-32607) is likewise gratefully acknowledged.

LITERATURE CITED

Abkarian M, Faivre M, Horton R, Smistrup K, Best-Popescu CA, Stone HA. 2008. Cellular-scale hydrodynamics. *Biomed. Mater.* 3:034011

Aidun CK, Clausen JR. 2010. Lattice-Boltzmann method for complex flows. *Annu. Rev. Fluid Mech.* 42:439–72

Aris R. 1962. *Vectors, Tensors, and the Basic Equations of Fluid Mechanics*. London: Prentice-Hall

Arroyo M, DeSimone A. 2009. Relaxation dynamics of fluid membranes. *Phys. Rev. E* 79:031915

Barthès-Biesel D, Rallison JM. 1981. The time-dependent deformation of a capsule freely suspended in a linear shear flow. *J. Fluid Mech.* 113:251–67

Biros G, Ying L, Zorin D. 2003. A fast solver for the Stokes equations with distributed forces in complex geometries. *J. Comput. Phys.* 193:317–48

Boal DH, Seifert U, Zilker A. 1992. Dual network model for red blood cell membranes. *Phys. Rev. Let.* 69:3405–8

Brady JF, Bossis G. 1988. Stokesian dynamics. *Annu. Rev. Fluid Mech.* 20:111–57

Bronkhorst PJH, Streekstra GJ, Grimbergen J, Nijhof EJ, Sixma JJ, Brakenhoff GJ. 1995. A new method to study shape recovery of red blood cells using multiple optical trapping. *Biophys. J.* 69:1666–73

Burns JM, Yang X, Forouzan O, Sosa JM, Shevkoplyas SS. 2012. Artificial microvascular network: a new tool for measuring rheologic properties of stored red blood cells. *Transfusion* 52:1010–23

Canuto C, Hussaini MY, Quarteroni A, Zang TA. 1987. *Spectral Methods in Fluid Dynamics*. Berlin: Springer-Verlag

Chang TMS. 2010. Blood replacement with nanobiotechnologically engineered hemoglobin and hemoglobin nanocapsules. *Wiley Intersci. Rev. Nanomed. Nanobiotechnol.* 2:418–30

Chang W, Giraldo F, Perot B. 2002. Analysis of an exact fractional step method. *J. Comput. Phys.* 180:183–99

Cheng H, Greengard L, Rokhlin V. 1999. A fast adaptive multipole algorithm in three dimensions. *J. Comput. Phys.* 55:468–98

Chien S. 1987. Red cell deformability and its relevance to blood flow. *Annu. Rev. Physiol.* 49:177–92

Cokelet GR. 1980. Rheology and hemodynamics. *Annu. Rev. Physiol.* 42:311–24

Cokelet GR, Meiselman HJ. 1968. Rheological comparison of hemoglobin solutions and erythrocyte suspensions. *Science* 162:275–77

Cox RG, Mason SG. 1972. Suspended particles in fluid flow through tubes. *Annu. Rev. Fluid Mech.* 13:291–316

Dao M, Li J, Suresh S. 2006. Molecularly based analysis of deformation of spectrin network and human erythrocyte. *Mater. Sci. Eng. C* 26:1232–44

Dao M, Lim CT, Suresh S. 2003. Mechanics of the human red blood cell deformed by optical tweezers. *J. Mech. Phys. Solids* 51:2259–80

Darden T, York D, Pedersen L. 1993. Particle mesh Ewald: an n log(n) method for Ewald sums in large systems. *J. Chem. Phys.* 98:10089–92

Dasi LP, Simon HA, Sucosky P, Yoganathan AP. 2009. Fluid mechanics of artificial heart valves. *Clin. Exp. Pharmacol. Physiol.* 36:225–37

Deplaine G, Safeukui I, Jeddi F, Lacoste F, Brousse V, et al. 2011. The sensing of poorly deformable red blood cells by the human spleen can be mimicked in vitro. *Blood* 117:e88–95

Deutsch S, Tarbell JM, Manning KB, Rosenberg G, Fontaine AA. 2006. Experimental fluid mechanics of pulsatile artificial blood pumps. *Annu. Rev. Fluid Mech.* 38:65–86

Dimitrakopoulos P. 2007. Interfacial dynamics in Stokes flow via a three-dimensional fully-implicit interfacial spectral boundary element algorithm. *J. Comput. Phys.* 225:408–26

Ding EJ, Aidun CK. 2003. Extension of the lattice-Boltzmann method for direct simulation of suspended particles near contact. *J. Stat. Phys.* 112:695–703

Discher DE, Boey SK, Boal DH. 1998. Simulations of the erythrocyte cytoskeleton at large deformation. II. Micropipette aspiration. *Biophys. J.* 75:1584–97

Discher DE, Mohandas N, Evans EA. 1994. Molecular maps of red-cell deformation: hidden elasticity and in situ connectivity. *Science* 266:1032–35

Doddi SK, Bagchi P. 2009. Three-dimensional computational modeling of multiple deformable cells flowing in microvessels. *Phys. Rev. E* 79:046318

Dodson WR III, Dimitrakopoulos P. 2012. Tank-treading of swollen erythrocytes in shear flows. *Phys. Rev. E* 85:021922

Durlofsky L, Brady JF, Bossis G. 1987. Dynamic simulation of hydrodynamically interacting particles. *J. Fluid Mech.* 180:21–49

Evans EA. 1983. Bending elastic modulus of red blood cell membrane derived from buckling instability in micropipet aspiration tests. *Biophys. J.* 43:27–30

Evans EA, Hochmuth RM. 1976a. Membrane viscoelasticity. *Biophys. J.* 16:1–11

Evans EA, Hochmuth RM. 1976b. Membrane viscoplastic flow. *Biophys. J.* 16:13–26

Evans EA, La Celle PA. 1975. Intrinsic material properties of the erythrocyte membrane indicated by mechanical analysis of deformation. *Blood* 45:29–43

Evans EA, Waugh R. 1977. Osmotic correction to elastic area compressibility measurements on red cell membrane. *Biophys. J.* 20:307–13

Fåhræus R, Lindqvist T. 1931. The viscosity of the blood in narrow capillary tubes. *Am. J. Physiol.* 96:562–68

Fedosov DA, Caswell B, Karniadakis GE. 2010. A multiscale red blood cell model with accurate mechanics, rheology, and dynamics. *Biophys. J.* 98:2215–25

Fedosov DA, Lei H, Caswell B, Suresh S, Karniadakis GE. 2012. Multiscale modeling of red blood cell mechanics and blood flow in malaria. *PLoS Comput. Biol.* 7:e1002270

Freund JB. 2002. Electro-osmosis in a nanometer-scale channel studied by atomistic simulation. *J. Chem. Phys.* 116:2194–200

Freund JB. 2007. Leukocyte margination in a model microvessel. *Phys. Fluids* 19:023301

Freund JB. 2013. The flow of red blood cells through a narrow spleen-like slit. *Phys. Fluids.* In press

Freund JB, Orescanin MM. 2011. Cellular flow in a small blood vessel. *J. Fluid Mech.* 671:466–90

Freund JB, Shapiro B. 2012. Transport of particles by magnetic forces and cellular blood flow in a model microvessel. *Phys. Fluids* 24:051904

Gompper G, Ihle T, Kroll DM, Winkler RG. 2008. Multi-particle collision dynamics: a particle-based mesoscale simulation approach to the hydrodynamics of complex fluids. In *Advanced Computer Simulation Approaches for Soft Matter Sciences III*, ed. C Holm, K Kremer, pp. 1–87. Adv. Polym. Sci. 221. Berlin: Springer-Verlag

Greengard L. 1988. *The Rapid Evaluation of Potential Fields in Particle Systems*. Cambridge, MA: MIT Press

Greengard L, Rokhlin V. 1987. A fast algorithm for particle simulations. *J. Comput. Phys.* 73:325–48

Guazzelli E, Morris JG. 2012. *A Physical Introduction to Suspension Dynamics*. Cambridge, UK: Cambridge Univ. Press

Guckel EK. 1997. *A P^3M method for calculation of Stokes interactions*. Master's thesis. Univ. Illinois Urbana-Champaign

Guido S, Tomaiuolo G. 2009. Microconfined flow behavior of red blood cells in vitro. *C. R. Phys.* 10:751–63

Han X, van Berkel C, Gwyer J, Capretto L, Morgan H. 2012. Microfluidic lysis of human blood for leukocyte analysis using single cell impedance cytometry. *Anal. Chem.* 84:1070–75

Happel J, Brenner H. 1965. *Low Reynolds Number Hydrodynamics*. London: Prentice-Hall

Hartmann D. 2010. A multiscale model for red blood cell mechanics. *Biomech. Model. Mechanobiol.* 9:1–17

Hashimoto H. 1959. On the periodic fundamental solutions of the Stokes equations and their application to viscous flow past a cubic array of cylinders. *J. Fluid Mech.* 5:317–28

Heinrich V, Ritchie K, Mohandas N, Evans E. 2001. Elastic thickness compressibilty of the red cell membrane. *Biophys. J.* 81:1452–63

Higgins JM, Eddington DT, Bhatia SN, Mahadevan L. 2009. Statistical dynamics of flowing red blood cells by morphological image processing. *PLoS Comput. Biol.* 5:e1000288

Higuera FJ, Jiménez J. 1989. Boltzmann approach to lattice gas simulations. *Europhys. Lett.* 9:663–68

Hochmuth RM, Mohandas N, Blackshear PL Jr. 1973. Measurement of the elastic modulus for red cell membrane using a fluid mechanical technique. *Biophys. J.* 13:747–62

Hochmuth RM, Ting-Beall HP, Beaty BB, Needham D, Tran-Son-Tay R. 1993. Viscosity of passive human neutrophils undergoing small deformations. *Biophys. J.* 54:1596–601

Hochmuth RM, Waugh RE. 1987. Erythrocyte membrane elasticity and viscosity. *Annu. Rev. Physiol.* 49:209–19

Hockney RW, Eastwood JW. 1988. *Computer Simulation Using Particles*. Bristol: Inst. Phys.

Homsy A, van der Wal PD, Doll W, Schaller R, Korsatko S, et al. 2012. Development and validation of a low cost blood filtration element separating plasma from undiluted whole blood. *Biomicrofluidics* 6:012804

Hoogerbrugge PJ, Koelman JMVA. 1992. Simulating microscopic hydrodynamic phenomena with dissipative particle dynamics. *Europhys. Lett.* 19:155–60

Humphrey JD. 2002. *Cardiovascular Solid Mechanics: Cells, Tissues, and Organs*. New York: Springer

Jackson SP, Nesbitt WS, Westein E. 2009. Dynamics of platelet thrombus formation. *J. Thromb. Haemost.* 7:17–20

Kamm RD. 2002. Cellular fluid mechanics. *Annu. Rev. Fluid Mech.* 34:211–32

Kim J, Massoudi M, Antaki JF, Gandini A. 2012. Removal of malaria-infected red blood cells using magnetic cell separators: a computational study. *Appl. Math. Comput.* 218:6841–50

Kim J, Moin P. 1985. Application of a fractional-step method to incompressible Navier-Stokes equations. *J. Comput. Phys.* 59:308–23

Kim S, Karrila SJ. 1991. *Microhydrodynamics: Principles and Selected Applications*. Boston: Butterworth-Heinemann

Koumoutsakos P. 2005. Multiscale flow simulations using particles. *Annu. Rev. Fluid Mech.* 37:457–87

Koumoutsakos P, Pivkin I, Milde F. 2013. The fluid mechanics of cancer and its therapy. *Annu. Rev. Fluid Mech.* 45:325–55

Krasik EF, Caputo KE, Hammer DA. 2008. Adhesive dynamics simulation of neutrophil arrest with stochastic activation. *Biophys. J.* 95:1716–28

Kravchenko AG, Moin P. 1997. On the effect of numerical errors in large eddy simulations of turbulent flows. *J. Comput. Phys.* 131:310–22

Kumar A, Graham MD. 2012a. Accelerated boundary integral method for multiphase flow in non-periodic geometries. *J. Comput. Phys.* 231:6682–713

Kumar A, Graham MD. 2012b. Mechanism of margination in confined flows of blood and other multicomponent suspensions. *Phys. Rev. Let.* 109:108102

Kwok WY, Moser RD, Jiménez J. 2001. A critical evaluation of the resolution properties of B-spline and compact finite difference methods. *J. Comput. Phys.* 174:510–51

Ladd AJC, Verberg R. 2001. Lattice-Boltzmann simulations of particle-fluid suspensions. *J. Stat. Phys.* 104:1191–251

Ladyzhenskaya OA. 1969. *The Mathematical Theory of Viscous Incompressible Flow*. New York: Gordon & Breach

Lambert CG, Darden TA, Board JA Jr. 1996. A multipole-based algorithm for efficient calculation of forces and potentials in macroscopic periodic assemblies of particles. *J. Comput. Phys.* 126:274–85

Layton BE, Lynch B, Peter T, Jamieson B. 2012. Red blood cell sorting with a multi-bed microfabricated filter. *J. Micromech. Microeng.* 22:025009

Leal LG. 1980. Particle motions in a viscous fluid. *Annu. Rev. Fluid Mech.* 12:435–76

LeVeque RJ, Li Z. 2003. Immersed interface methods for Stokes flow with elastic boundaries or surface tension. *SIAM J. Sci. Comput.* 18:709–35

Li J, Dao M, Lim CT, Suresh S. 2005. Spectrin-level modeling of the cytoskeleton and optical tweezers stretching of the erythrocyte. *Biophys. J.* 88:3707–19

Li Z, Ito K, Lai MC. 2007. An augmented approach for Stokes equations with a discontinuous viscosity and singular forces. *Comput. Fluids* 36:622–35

Linderkamp O, Meiselman HJ. 1982. Geometric, osmotic, and membrane mechanical properties of density-separated human red cells. *Blood* 59:1121–27

Linss W, Pilgrim C, Feuerstein H. 1991. How thick is the glycocalyx of human erythrocytes? *Acta Histochem.* 91:101–4

Lipowsky HH. 2005. Microconfined flow behavior of red blood cells in vitro. *Microcirculation* 12:5–15

MacMeccan RM, Clausen JR, Neitzel GP, Aidun CK. 2009. Simulating deformable particle suspensions using a coupled lattice-Boltzmann and finite-element method. *J. Fluid Mech.* 618:13–39

Marella SV, Udaykumar HS. 2004. Computational analysis of the deformability of leukocytes modeled with viscous and elastic structural components. *Phys. Fluids* 16:244–64

Mayerich D, Kwon J, Sung C, Abbott L, Keyser J, Choe Y. 2011. Fast macro-scale transmission imaging of microvascular networks using KESM. *Biomed. Opt. Express* 2:2888–96

Melrose JR, Ball RC. 1995. The pathological behaviour of sheared hard spheres with hydrodynamic interactions. *Europhys. Lett.* 32:535–40

Metsi E. 2000. *Large scale simulations of bidisperse emulsions and foams*. PhD thesis. Univ. Illinois Urbana-Champaign

Mills JP, Qie L, Dao M, Lim CT, Suresh S. 2004. Nonlinear elastic and viscoelastic deformation of the human red blood cell with optical tweezers. *Mech. Chem. Biosyst.* 1:169–80

Mittal R, Iaccarino G. 2005. Immersed boundary methods. *Annu. Rev. Fluid Mech.* 37:239–61

Mody NA, King MR. 2008. Platelet adhesive dynamics. *Biophys. J.* 95:2539–74

Mohandas N, Evans E. 1994. Mechanical properties of the red cell membrane in relation to molecular structure and genetic defects. *Annu. Rev. Biophys. Biomol. Struct.* 23:787–818

Moin P. 2010. *Fundamentals of Engineering Numerical Analysis*. Cambridge, UK: Cambridge Univ. Press. 2nd ed.

Moin P, Mahesh K. 1998. Direct numerical simulation: a tool in turbulence research. *Annu. Rev. Fluid Mech.* 30:539–78

Muldowney GP, Higdon JJL. 1995. A spectral boundary element approach to three-dimensional Stokes flow. *J. Fluid Mech.* 298:167–92

Nans A, Mohandas N, Stokes DL. 2011. Native ultrastructure of the red cell cytoskeleton by cryo-electron tomography. *Biophys. J.* 101:2341–50

Nguyen NQ, Ladd AJC. 2002. Lubrication corrections for lattice-Boltzmann simulations of particle suspensions. *Phys. Rev. E* 66:046708

Noguchi H, Gompper G. 2005. Shape transitions of fluid vesicles and red blood cells in capillary flows. *Proc. Natl. Acad. Sci. USA* 102:14159–64

Nunan KC, Keller JB. 1984. Effective viscosity of a periodic suspension. *J. Fluid Mech.* 142:269–87

Odqvist FHG. 1930. Über die randwertaufgaben der hydrodynamik zäther flüssigkeiten. *Math Z.* 32:329–75
Ogden RW. 1997. *Non-Linear Elastic Deformations*. New York: Dover
Pan W, Fedosov DA, Caswell B, Karniadakis GE. 2011. Predicting dynamics and rheology of blood flow: a comparative study of multiscale and low-dimensional models of red blood cells. *Microvasc. Res.* 82:163–70
Park YK, Best CA, Badizadegana K, Dasaria RR, Feld MS, et al. 2010. Measurement of red blood cell mechanics during morphological changes. *Proc. Natl. Acad. Sci. USA* 107:6731–36
Pivkin IV, Karniadakis GE. 2008. Accurate coarse-grained modeling of red blood cells. *Phys. Rev. Let.* 101:118105
Pollock E, Glosli J. 1996. Comments on PPPM, FMM, and the Ewald method for large periodic Coulombic systems. *Comput. Phys. Commun.* 95:93–110
Popel AS. 1989. Theory of oxygen transport to tissue. *Crit. Rev. Biomed. Eng.* 17:257–321
Popel AS, Johnson PC. 2005. Microcirculation and hemorheology. *Annu. Rev. Fluid Mech.* 37:43–69
Pozrikidis C. 1992. *Boundary Integral and Singularity Methods for Linearized Viscous Flow*. Cambridge, UK: Cambridge Univ. Press
Pozrikidis C. 2001. Interfacial dynamics for Stokes flow. *J. Comput. Phys.* 169:250–301
Pozrikidis C. 2005. Axisymmetric motion of a file of red blood cells through capillaries. *Phys. Fluids* 17:031503
Pozrikidis C. 2009. Numerical simulation of blood flow through microvascular capillary networks. *Bull. Math. Biol.* 71:1520–41
Pries AR, Neuhaus D, Gaehtgens P. 1992. Blood viscosity in tube flow: dependence on diameter and hematocrit. *Am. J. Physiol. Heart Circ. Physiol.* 263:H1770–78
Puig-de-Morales-Marinkovic M, Turner KT, Butler JP, Fredberg JJ, Suresh S. 2007. Viscoelasticity of the human red blood cell. *Am. J. Physiol. Cell Physiol.* 293:C597–605
Rahimian A, Lashuk I, Veerapaneni SK, Chandramowlishwaran A, Malhotra D, et al. 2010. Petascale direct numerical simulation of blood flow on 200K cores and heterogeneous architectures. *SC '10: Proc. 2010 ACM/IEEE Int. Conf. High-Perform. Comput. Netw. Storage Anal.* Washington, DC: IEEE Comput. Soc. doi: 10.1109/SC.2010.42
Rallison JM, Acrivos A. 1978. A numerical study of the deformation and burst of a viscous drop in an extensional flow. *J. Fluid Mech.* 89:191–200
Reasor DA Jr, Clausen JR, Aidun CK. 2012. Coupling the lattice-Boltzmann and spectrin-link methods for the direct numerical simulation of cellular blood flow. *Int. J. Numer. Methods Fluids* 68:767–81
Saintillan D, Darve E, Shaqfeh ESG. 2005. A smooth particle-mesh Ewald algorithm for Stokes suspension simulations: the sedimentation of fibers. *Phys. Fluids* 17:033301
Sangania AS, Mo G. 1996. An $O(N)$ algorithm for Stokes and Laplace interactions of particles. *Phys. Fluids* 8:1990–2010
Schmid-Schönbein GW. 2006. Analysis of inflammation. *Annu. Rev. Biomed. Eng.* 8:93–151
Secomb TW. 2003. Mechanics of red blood cells and blood flow in narrow tubes. In *Modeling and Simulation of Capsules and Biological Cells*, ed. C Pozrikidis, pp. 163–96. Boca Raton, FL: Chapman & Hall/CRC
Secomb TW, Beard DA, Frisbee JC, Smith NP, Pries AR. 2008. The role of theoretical modeling in microcirculation. *Microcirculation* 15:693–98
Secomb TW, Skalak R. 1982. Surface flow of viscoelastic membranes in viscous fluids. *Q. J. Mech. Appl. Math.* 35:233–47
Secomb TW, Skalak R, Ozkaya N, Gross JF. 1986. Flow of axisymmetrical red blood cells in narrow capillaries. *J. Fluid Mech.* 163:405–23
Selmi H, Elasmi L, Ghigliotti G, Misbah C. 2011. Boundary integral and fast multipole method for two dimensional vesicle sets in Poiseuille flow. *Discrete Contin. Dyn. Syst. B* 15:1065–76
Sierou A, Brady JF. 2001. Accelerated Stokesian dynamics simulations. *J. Fluid Mech.* 448:115–46
Skalak R, Ozkaya N, Skalak TC. 1989. Biofluid mechanics. *Annu. Rev. Fluid Mech.* 21:167–204
Skalak R, Tozeren A, Zarda RP, Chien S. 1973. Strain energy function of red blood cell membranes. *Biophys. J.* 13:245–80
Stickel JJ, Powell RL. 2005. Fluid mechanics and rheology of dense suspensions. *Annu. Rev. Fluid Mech.* 37:129–49
Sun C, Munn LL. 2008. Lattice-Boltzmann simulation of blood flow in digitized vessel networks. *Comput. Math. Appl.* 55:1594–600

Suresh S. 2006. Mechanical response of human red blood cells in health and disease: some structure-property-function relationships. *J. Mater. Res.* 21:1871–77

Toner M, Irimia D. 2005. Blood-on-a-chip. *Annu. Rev. Biomed. Eng.* 7:77–103

Tornberg AK, Greengard L. 2008. A fast multipole method for the three-dimensional Stokes equations. *J. Comput. Phys.* 227:1613–19

Veerapaneni SK, Rahimian A, Biros G, Zorin D. 2011. A fast algorithm for simulating vesicle flows in three dimensions. *J. Comput. Phys.* 230:5610–34

Vigmostad SC, Udaykumar HS, Lu J, Chandran KB. 2010. Fluid-structure interaction methods in biological flows with special emphasis on heart valve dynamics. *Int. J. Numer. Methods Biomed. Eng.* 26:435–70

Waugh R, Evans EA. 1979. Thermoelasticity of red blood cell membrane. *Biophys. J.* 26:115–32

Weinbaum S, Tarbell JM, Damiano ER. 2007. The structure and function of the endothelial glycocalyx layer. *Annu. Rev. Biomed. Eng.* 9:121–67

Wetzel B, Schaefer H. 1982. Scanning electron microscope image of blood cells. AV-8202-3656. Natl. Cancer Inst., Bethesda, MD. **http://visualsonline.cancer.gov/details.cfm?imageid=2129**

Xu H, Sagaut P. 2011. Optimal low-dispersion low-dissipation LBM schemes for computational aeroacoustics. *J. Comput. Phys.* 230:5353–82

Xu S. 2008. The immersed interface method for simulating prescribed motion of rigid objects in an incompressible viscous flow. *J. Comput. Phys.* 227:5045–71

Yang S, Lee SS, Ahn SW, Kang K, Shim W, et al. 2012. Deformability-selective particle entrainment and separation in a rectangular microchannel using medium viscoelasticity. *Soft Matter* 8:5011–19

Yazdani AZK, Bagchi P. 2011. Phase diagram and breathing dynamics of a single red blood cell and a biconcave capsule in dilute shear flow. *Phys. Rev. E* 84:236314

Yoon YZY, Kotar J, Yoon G, Cicuta P. 2008. The nonlinear mechanical response of the red blood cell. *Phys. Biol.* 5:036007

Youngren GK, Acrivos A. 1975. Stokes flow past a particle of arbitrary shape: a numerical method of solution. *J. Fluid Mech.* 69:377–403

Zhao H, Isfahani AHG, Olson L, Freund JB. 2010. A spectral boundary integral method for flowing blood cells. *J. Comput. Phys.* 229:3726–44

Zhao H, Shaqfeh ESG, Narsimhan V. 2012. Shear-induced particle migration and margination in a cellular suspension. *Phys. Fluids* 24:011902

Zick AA, Homsy GM. 1982. Stokes flow through periodic arrays of spheres. *J. Fluid Mech.* 115:13–26

Zinchenko AZ, Davis RH. 2000. An efficient algorithm for hydrodynamical interaction of many deformable drops. *J. Comput. Phys.* 157:539–87